

A Complete Classification of Sub-Shocks in the Shock Structure of a Binary Mixture of Eulerian Gases with Different Degrees of Freedom

Tomaso Ruggeri¹ and Shigeru Taniguchi²

¹⁾*Department of Mathematics & Alma Mater Research Center on Applied Mathematics, University of Bologna, Bologna, Italy*

²⁾*Department of Creative Engineering, National Institute of Technology, Kitakyushu College, Kitakyushu, Japan*

(*Electronic mail: tommaso.ruggeri@unibo.it)

(*Electronic mail: taniguchi.shigeru@kct.ac.jp)

(Dated: 11 April 2022)

The shock structure in a binary mixture of polyatomic Eulerian gases with different degrees of freedom of a molecule is studied based on the multi-temperature model of rational extended thermodynamics. Since the system of field equations is hyperbolic, the shock-structure solution is not always regular, and discontinuous parts (sub-shocks) can be formed. For given values of the mass ratio and the specific heats of the constituents, we identify the possible sub-shocks as the Mach number M_0 of the shock wave and the concentration c of the constituents change. In the plane (c, M_0) , we identify the possible regions for the sub-shock formation. The analysis is obtained to verify when the velocity of the shock wave meets a characteristic velocity in the unperturbed or perturbed equilibrium states that gives a necessary condition for the sub-shock formation. The condition becomes necessary and sufficient when the velocity of the shock becomes greater than the maximum characteristic velocity in the unperturbed state. Namely, the regions with no sub-shocks, a sub-shock for only one constituent, or sub-shocks for both constituents are comprehensively classified. The most interesting case is that the lighter molecule has more degrees of freedom than that of the heavy one. In this situation, the topology of the various regions becomes different. We also solve the system of the field equations numerically using the parameters in the various regions and confirm whether the sub-shocks emerge or not. Finally, the relationship between an acceleration wave in a constituent and the sub-shock in the other constituent is explicitly derived.

I. INTRODUCTION

The shock wave phenomenon has attracted many researchers in various fields because of its wide-range applications^{1,2}. An up-to-date survey of the shock waves based on the hyperbolic theories can be found in a review paper³ and from the mathematical point of view in the recent book of Liu⁴. One of the essential differences from the parabolic theory is that the hyperbolic theory does not always predict a continuous solution of the shock structure, and a discontinuous part (sub-shock) may appear depending on the velocity s of the shock wave. Ruggeri showed that the shock-structure solution becomes, in principle, singular when s meets any characteristic velocity of the hyperbolic system⁵. Boillat and Ruggeri proved a theorem⁶ stating that if the hyperbolic system of balance laws has a convex entropy, a continuous solution for the shock structure cannot exist when s is greater than the maximum characteristic velocity evaluated in the equilibrium state in front of the shock wave and a sub-shock arises. The possibility of the sub-shock formation with smaller s than the maximum characteristic velocity is still unclear. In the theory of Rational Extended Thermodynamics (RET) of a monatomic gas⁷, Weiss proved numerically that when s meets the characteristic velocity, the solution becomes regular except for the maximum characteristic velocity evaluated in the unperturbed state in accordance with the Boillat-Ruggeri theorem⁸. For this reason, it has been conjectured that the sub-shock can appear only when s is greater than the maximum characteristic velocity. This conjecture has also been confirmed for single polyatomic gases^{9–11}. Recently, by adopting several hyper-

bolic systems of field equations, counter-examples of this conjecture have also been found in the context of a mixture of rarefied monatomic gas^{12–14} and also of simple toy models^{9,15}.

In order to understand the nature of the sub-shock formation more deeply, we focus on the shock structure in a binary mixture of polyatomic Eulerian gases¹⁶, which is modeled in the spirit of RET theory. For small Mach numbers (weak shocks), no sub-shock arises, as was proved in the case of a binary mixture of monatomic gases^{17,18}. A comparison with the experimental results was also made, and this analysis shows good agreement between the theoretical prediction and experimental data on the mass density¹⁹. In the present analysis, we want to consider also strong shocks in a binary mixture of polyatomic gases with different degrees of freedom, and we want to give also a comparison with the results obtained in a binary mixture of monatomic gases^{11,12}.

In the previous paper²⁰, preliminary results of the sub-shock formation in a binary mixture of rarefied polyatomic gases are summarized, and the shock structure with multiple sub-shocks is shown when the degrees of freedom of a heavier molecule are larger or equal to the degrees of freedom of a lighter molecule. In the present paper, a complete classification of the sub-shock formation will be made with particular attention to the case with smaller degrees of freedom of the lighter molecule than the degrees of freedom of the heavy one. In these last circumstances, we show that a more complicated and interesting situation arises for the regions of possible sub-shocks formation varying the Mach number and the concentration of the two species for an assigned ratio of mass and prescribed degree of freedoms.

The organization of the present paper is summarized as follows. In section II, the balance laws system and the constitutive equations are summarized. We adopt a multi-temperature Eulerian model of a binary mixture of rarefied gases in which the entropy inequality is satisfied, and the entropy density is a convex function (thermodynamical stability). The shock structure problem is explained in section III, and we classify possible regions from the viewpoint of the necessary conditions for the sub-shock formation in section IV. Section V is devoted to the confirmation of all possible cases by solving numerical field equations. Moreover, we prove that an acceleration wave appears in a constituent when the sub-shock emerges in the other constituent. Furthermore, the profiles of the average temperature are also shown. The summary and concluding remarks will be shown in section VI.

II. BASIC EQUATIONS

We consider a binary mixture of rarefied polytropic gases described by the following thermal and caloric equations of state:

$$p_\alpha = \frac{k_B}{m_\alpha} \rho_\alpha T_\alpha, \quad \varepsilon_\alpha = \frac{1}{\gamma_\alpha - 1} \frac{k_B}{m_\alpha} T_\alpha, \quad (1)$$

where k_B , p_α , m_α , ε_α , ρ_α and γ_α are, respectively, the Boltzmann constant, the pressure, the molecular mass, the specific internal energy, the mass density and the ratio of the specific heats of the species $\alpha = 1, 2$. The global pressure p and the global specific intrinsic internal energy ε_I are:

$$p = p_1 + p_2, \quad \rho \varepsilon_I = \rho_1 \varepsilon_1 + \rho_2 \varepsilon_2, \quad (2)$$

where ρ is the total mass density given by

$$\rho = \rho_1 + \rho_2. \quad (3)$$

In an equilibrium state where $T_1 = T_2 = T$ we can impose the same form of (1) on p^E and ε_I^E :

$$p^E = \rho \frac{k_B}{m} T, \quad \varepsilon_I^E = \frac{1}{\gamma - 1} \frac{k_B}{m} T \quad (4)$$

provided that we introduce the average mass $m \equiv m(c)$ and the average ratio of the specific heats $\gamma \equiv \gamma(c)$ of the mixture in the following form¹⁶:

$$\begin{aligned} \frac{1}{m(c)} &= \frac{c}{m_1} + \frac{1-c}{m_2}, \\ \frac{1}{\gamma-1} &= \frac{m(c)}{m_1} \frac{c}{\gamma_1-1} + \frac{m(c)}{m_2} \frac{1-c}{\gamma_2-1}, \end{aligned} \quad (5)$$

where c ($0 \leq c \leq 1$) is the concentration related to the mass densities:

$$\rho_1 = \rho c, \quad \rho_2 = \rho(1-c).$$

For the analysis of mixtures, it is convenient to introduce the diffusion velocity \mathbf{u}_α :

$$\mathbf{u}_\alpha = \mathbf{v}_\alpha - \mathbf{v}, \quad \left(\sum_{\alpha=1}^2 \rho_\alpha \mathbf{u}_\alpha = \mathbf{0} \right),$$

where the mixture velocity \mathbf{v} is defined by

$$\mathbf{v} = \frac{1}{\rho} \sum_{\alpha=1}^2 \rho_\alpha \mathbf{v}_\alpha \quad (6)$$

with \mathbf{v}_α being the velocity of the constituent α . We focus on the one-dimensional problem in the x -direction such that the velocities are expressed as

$$\mathbf{v} = (v, 0, 0), \quad \mathbf{v}_\alpha = (v_\alpha, 0, 0), \quad \mathbf{u}_\alpha = (u_\alpha, 0, 0).$$

Furthermore, it is assumed that chemical reactions are not present. Then the system of a mixture of Eulerian gases is^{11,16,21}:

$$\begin{aligned} \frac{\partial \rho_1}{\partial t} + \frac{\partial \rho_1 v_1}{\partial x} &= 0, \\ \frac{\partial \rho_1 v_1}{\partial t} + \frac{\partial}{\partial x} (\rho_1 v_1^2 + p_1) &= \hat{m}_1, \\ \frac{\partial}{\partial t} (\rho_1 v_1^2 + 2\rho_1 \varepsilon_1) + \frac{\partial}{\partial x} \{ (\rho_1 v_1^2 + 2\rho_1 \varepsilon_1 + 2p_1) v_1 \} &= 2(\hat{e}_1 + \hat{m}_1 v), \\ \frac{\partial \rho_2}{\partial t} + \frac{\partial \rho_2 v_2}{\partial x} &= 0, \\ \frac{\partial \rho_2 v_2}{\partial t} + \frac{\partial}{\partial x} (\rho_2 v_2^2 + p_2) &= \hat{m}_2, \\ \frac{\partial}{\partial t} (\rho_2 v_2^2 + 2\rho_2 \varepsilon_2) + \frac{\partial}{\partial x} \{ (\rho_2 v_2^2 + 2\rho_2 \varepsilon_2 + 2p_2) v_2 \} &= 2(\hat{e}_2 + \hat{m}_2 v). \end{aligned} \quad (7)$$

The production terms \hat{m}_α and \hat{e}_α represent the interchange of the momentum and the energy, respectively, and we have to take

into account the following relations:

$$\sum_{\alpha=1}^2 \hat{m}_\alpha = \sum_{\alpha=1}^2 \hat{e}_\alpha = 0.$$

The system (7) is equivalent to the following system^{11,16,21}:

$$\begin{aligned} \frac{\partial \rho}{\partial t} + \frac{\partial \rho v}{\partial x} &= 0, \\ \frac{\partial \rho v}{\partial t} + \frac{\partial}{\partial x} (\rho v^2 + p + \Pi - \sigma) &= 0, \\ \frac{\partial}{\partial t} \left(\frac{1}{2} \rho v^2 + \rho \varepsilon \right) + \frac{\partial}{\partial x} \left\{ \left(\frac{1}{2} \rho v^2 + \rho \varepsilon + p + \Pi - \sigma \right) v + q \right\} &= 0, \\ \frac{\partial \rho_1}{\partial t} + \frac{\partial \rho_1 v_1}{\partial x} &= 0, \\ \frac{\partial \rho_1 v_1}{\partial t} + \frac{\partial}{\partial x} (\rho_1 v_1^2 + p_1) &= \hat{m}_1, \\ \frac{\partial}{\partial t} (\rho_1 v_1^2 + 2\rho_1 \varepsilon_1) + \frac{\partial}{\partial x} \{ (\rho v_1^2 + 2\rho_1 \varepsilon_1 + 2p_1) v_1 \} &= 2(\hat{e}_1 + \hat{m}_1 v), \end{aligned} \quad (8)$$

where in the one-dimensional case the deviatoric part of the global shear stress σ , the global dynamic pressure Π , the global specific internal energy ε and the global heat flux q are given by

$$\begin{aligned} \sigma &= -\frac{2}{3} \sum_{\alpha=1}^2 \rho_\alpha u_\alpha^2 = -\frac{2}{3} \frac{\rho_1 \rho}{\rho_2} u_1^2, \\ \Pi &= \sum_{\alpha=1}^2 \frac{1}{3} \rho_\alpha u_\alpha^2 = -\frac{\sigma}{2}, \\ \rho \varepsilon &= \rho \varepsilon_I + \frac{1}{2} \sum_{\alpha=1}^2 \rho_\alpha u_\alpha^2 = \rho \varepsilon_I + \frac{1}{2} (\Pi - \sigma), \\ q &= \sum_{\alpha=1}^2 \left(\frac{1}{2} \rho_\alpha u_\alpha^2 + \rho_\alpha \varepsilon_\alpha + p_\alpha \right) u_\alpha, \end{aligned} \quad (9)$$

and the global p and intrinsic energy ε_I are given by (2).

The system (8) is compatible with the supplementary entropy law¹⁶:

$$\frac{\partial h}{\partial t} + \frac{\partial k}{\partial x} = \Sigma, \quad (10)$$

where h and k are, respectively, the entropy density and the entropy flux, and the entropy production Σ is given by

$$\Sigma = \hat{m}_1 \hat{\Lambda}^{v_1} + \hat{e}_1 (2\hat{\Lambda}^{\varepsilon_1})$$

with $\hat{\Lambda}^{v_1}$ and $\hat{\Lambda}^{\varepsilon_1}$ being the components of the Lagrange multipliers (*main field*) evaluated in the rest frame relative to the last two balance laws in (8)¹⁶:

$$\hat{\Lambda}^{v_1} = -\frac{u_1}{T_1} + \frac{u_2}{T_2}, \quad \hat{\Lambda}^{\varepsilon_1} = \frac{1}{2T_1} - \frac{1}{2T_2}. \quad (11)$$

The expressions of \hat{m}_1 and \hat{e}_1 are obtained such that Σ is positive and quadratic as usual in non-equilibrium thermodynam-

ics:

$$\begin{aligned} \hat{m}_1 &= \psi \hat{\Lambda}^{v_1} = \psi \left(\frac{u_2}{T_2} - \frac{u_1}{T_1} \right), \\ \hat{e}_1 &= 2\theta \hat{\Lambda}^{\varepsilon_1} = \theta \left(\frac{1}{T_1} - \frac{1}{T_2} \right), \end{aligned} \quad (12)$$

where the phenomenological coefficients $\psi > 0$ and $\theta > 0$ depend on the mass densities and temperatures. Their functional forms may be determined by kinetic theoretical consideration and/or experimental data.

Inserting the constitutive equations (1) and the production terms (12) into the system (7) or the equivalent system (8), we obtain a closed system with the unknown $(\rho_1, v_1, T_1, \rho_2, v_2, T_2)$ or $(\rho, v, T, \rho_1, v_1, T_1)$. It is noticeable that there appear in the system (8) through (9) the global viscous stress σ , the dynamical pressure Π and the global heat flux q due to the diffusion of velocities and temperatures even if we neglect these dissipative quantities in the field equations for each constituent.

From (12) and (11), we have $v = v_1 = v_2$ and $T = T_1 = T_2$ in an equilibrium state from the condition that the production terms \hat{m}_1 and \hat{e}_1 vanish. The associate *equilibrium subsystem*²² of (8) is given by the four first equations of (8) with fields evaluate in equilibrium:

$$\begin{aligned} \frac{\partial \rho}{\partial t} + \frac{\partial \rho v}{\partial x} &= 0, \\ \frac{\partial \rho_1}{\partial t} + \frac{\partial \rho_1 v}{\partial x} &= 0, \\ \frac{\partial \rho v}{\partial t} + \frac{\partial}{\partial x} (\rho v^2 + p^E) &= 0, \\ \frac{\partial}{\partial t} \left(\frac{1}{2} \rho v^2 + \rho \varepsilon_I^E \right) + \frac{\partial}{\partial x} \left\{ \left(\frac{1}{2} \rho v^2 + \rho \varepsilon_I^E + p^E \right) v \right\} &= 0, \end{aligned} \quad (13)$$

where p^E and ε_I^E are the equilibrium pressure and the specific internal energy (2) with m and γ given in (5).

III. SHOCK STRUCTURE

The system of field equations (7), or equivalently (8), belongs to a particular case of general first order hyperbolic quasi-linear system of balance laws:

$$\frac{\partial \mathbf{u}}{\partial t} + \frac{\partial \mathbf{F}(\mathbf{u})}{\partial x} = \mathbf{P}(\mathbf{u}), \quad (14)$$

where \mathbf{u} , \mathbf{F} , and \mathbf{P} are column vectors of R^N representing the density, the flux, and the production, respectively.

The shock structure is described as a traveling-wave solution depending on a single variable $\varphi = x - st$, which asymptotically connects equilibrium states in front and behind the shock wave. Namely,

$$\mathbf{u} \equiv \mathbf{u}(\varphi), \quad \varphi = x - st \quad (15)$$

with constant equilibrium boundary conditions at infinity:

$$\lim_{\varphi \rightarrow +\infty} \mathbf{u} = \mathbf{u}_0, \quad \lim_{\varphi \rightarrow -\infty} \mathbf{u} = \mathbf{u}_I, \quad (16)$$

where

$$\mathbf{P}(\mathbf{u}_0) = \mathbf{P}(\mathbf{u}_I) = 0. \quad (17)$$

We call the equilibrium states \mathbf{u}_0 and the \mathbf{u}_I *unperturbed state* and *perturbed state*, respectively. Hereafter, the quantities with the subscript 0 represent the quantities evaluated in the unperturbed state, and the quantities with subscript I represent the ones evaluated in the perturbed state. By inserting (15) into (14), we have the following ODE system:

$$(\mathbf{A}(\mathbf{u}) - s\mathbf{I}) \frac{d\mathbf{u}}{d\varphi} = \mathbf{P}(\mathbf{u}), \quad \mathbf{A} = \frac{\partial \mathbf{F}}{\partial \mathbf{u}} \quad (18)$$

with boundary conditions given by (16).

As pointed out by Ruggeri⁶, when s meets a characteristic velocity λ , which is the eigenvalue of the matrix \mathbf{A} , the solution may have a breakdown, in other words, a singularity (sub-shock) may appear. In order to discuss the necessary condition for the sub-shock formation, we need to analyze the meeting points between s and λ .

Following⁶, by taking the typical features of rational extended thermodynamics into account, we may split the system (14) into the blocks of M conservation laws and of $N - M$ balance equations as follows ((8) belongs in this kind of system):

$$\begin{aligned} \frac{\partial \mathbf{V}(\mathbf{u})}{\partial t} + \frac{\partial \mathbf{R}(\mathbf{u})}{\partial x} &= 0, \\ \frac{\partial \mathbf{W}(\mathbf{u})}{\partial t} + \frac{\partial \mathbf{Q}(\mathbf{u})}{\partial x} &= \mathbf{g}(\mathbf{u}). \end{aligned} \quad (19)$$

Taking (19) and (15) into account, we may rewrite (18) as

$$\begin{aligned} \frac{d}{d\varphi} \{ -s\mathbf{V}(\mathbf{u}) + \mathbf{R}(\mathbf{u}) \} &= 0, \\ -s \frac{d\mathbf{W}(\mathbf{u})}{d\varphi} + \frac{d\mathbf{Q}(\mathbf{u})}{d\varphi} &= \mathbf{g}(\mathbf{u}). \end{aligned} \quad (20)$$

By integrating (20)₁, we have

$$-s\mathbf{V}(\mathbf{u}) + \mathbf{R}(\mathbf{u}) = \text{const.} \quad (21)$$

and in particular taking into account (16) we have

$$-s\mathbf{V}(\mathbf{u}_0) + \mathbf{R}(\mathbf{u}_0) = -s\mathbf{V}(\mathbf{u}_I) + \mathbf{R}(\mathbf{u}_I). \quad (22)$$

The conditions (22) is nothing else the Rankine-Hugoniot conditions of the equilibrium subsystem:

$$\frac{\partial \mathbf{V}(\mathbf{u})}{\partial t} + \frac{\partial \mathbf{R}(\mathbf{u})}{\partial x} = 0, \quad \mathbf{g}(\mathbf{u}) = 0. \quad (23)$$

For a given unperturbed state \mathbf{u}_0 , and the shock velocity s , one may determine the perturbed state \mathbf{u}_I as function of \mathbf{u}_0 , and the shock velocity s . Due to the Galilean invariance, we can choose the unperturbed velocity as $v_0 = 0$ without any loss of generality. Taking into account the conservation laws, we have the following boundary conditions:

$$\mathbf{u}_0 = \begin{bmatrix} \rho_0 \\ v_0 = 0 \\ T_0 \\ (\rho_1)_0 = c_0 \rho_0 \\ (v_1)_0 = v_0 = 0 \\ (T_1)_0 = T_0 \end{bmatrix}, \quad \mathbf{u}_I = \begin{bmatrix} \rho_I \\ v_I \\ T_I \\ (\rho_1)_I = c_1 \rho_I \\ (v_1)_I = v_I \\ (T_1)_I = T_I \end{bmatrix} \quad (24)$$

with $\sigma_0 = \Pi_0 = q_0 = \sigma_I = \Pi_I = q_I = 0$. We notice that the system (13) except for the second equation is the Euler system of a single fluid and therefore the RH conditions gives:

$$\begin{aligned} \rho_I &= \frac{(\gamma_0 + 1)M_0^2}{2 + (\gamma_0 - 1)M_0^2} \rho_0, & v_I &= \frac{2(M_0^2 - 1)}{(\gamma_0 + 1)M_0} a_0, \\ T_I &= \frac{\{2 + (\gamma_0 - 1)M_0^2\}\{1 + \gamma_0(2M_0^2 - 1)\}}{(\gamma_0 + 1)^2 M_0^2} T_0, \end{aligned} \quad (25)$$

with γ_0 being the function γ given in (5) evaluated in the unperturbed state $\gamma_0 = \gamma(c_0)$,

$$M_0 = \frac{s - v_0}{a_0} = \frac{s}{a_0}, \quad (26)$$

M_0 is the unperturbed Mach number, a_0 is the sound velocity in the unperturbed state

$$a_0 = \sqrt{\gamma_0 \frac{k_B}{m_0} T_0}$$

and m_0 is being the equilibrium average mass (5) evaluated in the unperturbed state: $m_0 = m(c_0)$. The RH equation for the second equation combined with the RH of the first equation of (13) give immediately that the concentration is the same in both equilibrium states $c_1 = c_0$, and in the sequel, it will be termed equilibrium concentration, without special regard to unperturbed or perturbed state.

IV. REGIONS CLASSIFIED BY THE POSSIBILITY OF SUB-SHOCK FORMATION

To analyze the regularity of the shock-structure solution in a binary mixture, we recall the characteristic velocities of the full system (7) in equilibrium in which both constituents have common velocity v and temperature T :

$$v \pm \sqrt{\gamma_1 \frac{k_B}{m_1} T}, \quad v \text{ (multiplicity 2)}, \quad v \pm \sqrt{\gamma_2 \frac{k_B}{m_2} T}. \quad (27)$$

The characteristic velocities of the equilibrium subsystem (13) are

$$v - \sqrt{\gamma \frac{k_B}{m} T}, \quad v \text{ (multiplicity 2)}, \quad v + \sqrt{\gamma \frac{k_B}{m} T},$$

where γ and m are given by (5).

We focus only on positive velocities with respect to the frame moving with the fluid as for symmetry the negative ones have the same properties. Let define the characteristic velocities in equilibrium of species 1 and 2:

$$\lambda_1 = v + \sqrt{\gamma_1 \frac{k_B}{m_1} T}, \quad \lambda_2 = v + \sqrt{\gamma_2 \frac{k_B}{m_2} T} \quad (28)$$

and we call

$$\bar{\lambda} = v + \sqrt{\gamma \frac{k_B}{m} T} \quad (29)$$

the characteristic velocity of the equilibrium subsystem. It is noticeable that the magnitude relation between the characteristic velocities for species 1 and 2 depends on the values of γ_1/m_1 and γ_2/m_2 . But by the Theorem²², the subcharacteristic conditions hold and we have

$$\bar{\lambda} \leq \max(\lambda_1, \lambda_2).$$

We consider the shock family that bifurcates from the trivial zero shock solution when $s = \bar{\lambda}_0$. In this case, by using the Lax condition²³, we can determine the admissibility and obtain the following admissible equilibrium states (24) $\bar{\lambda}_0 < s < \bar{\lambda}_1$. This conditions is equivalently expressed as $M_0 > 1$ as is expected. Hereafter we call species 1 the one with smaller or equal mass between the two species: $m_1 \leq m_2$. In order to classify the possible cases, we introduce the ratio of the masses of the constituents,

$$\mu = \frac{m_1}{m_2}, \quad (0 < \mu \leq 1),$$

and the ratio of the specific heats g ,

$$g = \frac{\gamma_1}{\gamma_2}.$$

Moreover we recall that the degree of freedom of a species D_α is related to the ratio of specific heats γ_α by the relation

$$D_\alpha = \frac{2}{\gamma_\alpha - 1}, \quad \alpha = 1, 2. \quad (30)$$

In the following, we consider the following two cases separately

$$\begin{aligned} \text{Case A : } & \gamma_1 \geq \gamma_2, \\ \text{Case B : } & \gamma_1 < \gamma_2, \end{aligned}$$

In Case A, the lighter species has fewer or equal degrees of freedom than the heavier, while in Case B, the species with smaller mass has more degrees of freedom than the species with larger mass.

To our knowledge, only the preliminary analysis of the case A was done; in particular, there are some results for mixtures of both monatomic gases ($\gamma_1 = \gamma_2 = 5/3$)^{12,13,18}, while the case B has never been studied at least for a complete classification of sub-shock formation.

A. Case A: $\gamma_1 \geq \gamma_2$

The preliminary results on the shock structure of Case A in a binary mixture of polyatomic gases were summarized in the previous paper²⁰. A binary mixture of monatomic gases in which $\gamma_1 = \gamma_2 = 5/3$, ($g = 1$) belong in this case.

In the Case A, the characteristic velocities in equilibrium in front the shock satisfies the inequalities for any $c_0 \in]0, 1[$ and any $\mu \in]0, 1[$:

$$\lambda_{20} < \bar{\lambda}_0 < \lambda_{10}, \quad s > \bar{\lambda}_0. \quad (31)$$

According to the Theorem proved in⁶, a sub-shock appears if the shock velocity is faster than the maximum characteristic velocity in the unperturbed state $s > \lambda_{10}$ and in the present case, we obtain the following condition:

$$M_0 > M_{10} = \frac{\lambda_{10}}{a_0} = \sqrt{\frac{m_0 \gamma_1}{m_1 \gamma_0}} = \sqrt{\frac{\gamma_1}{\gamma_0 \{c_0 + (1 - c_0)\mu\}}},$$

where M_{10} is the dimensionless characteristic velocity for the constituent 1 evaluated in the unperturbed state. Taking into account (5), it is easy to see that

$$\lim_{c_0 \rightarrow 1} M_{10} = 1.$$

As typical examples, the dependence of M_{10} on c_0 for $\mu = 0.45$, $\gamma_1 = 7/5$, and $\gamma_2 = 9/7$ is given in Figures 1 and 2. We see that if the parameters lie in the Regions III and IV of the figures, there exists a sub-shock involving the variables of the first constituent that we call S_1^A the index indicates the constituent 1 and A means that the sub-shock emerges after the maximum eigenvalues in the unperturbed state.

To know if other sub-shocks can exists we recall the observation that a sub-shock can arise when s meets an eigenvalue λ evaluated along with the shock structure (see (18)).

For the genuine-non linearity along the solution both $\lambda_2(\mathbf{u}(\varphi))$ and $\lambda_1(\mathbf{u}(\varphi))$ are increasing function of s ²⁴, and therefore taking into account (31), only $\lambda_2(\mathbf{u}^*) = s$ can be verified for some value of φ^* . As $\lambda_{20} \leq \lambda_2(\mathbf{u}^*) \leq \lambda_{21}$, a necessary condition (but not sufficient) is that $\lambda_{21}(s) > s$ that in term of

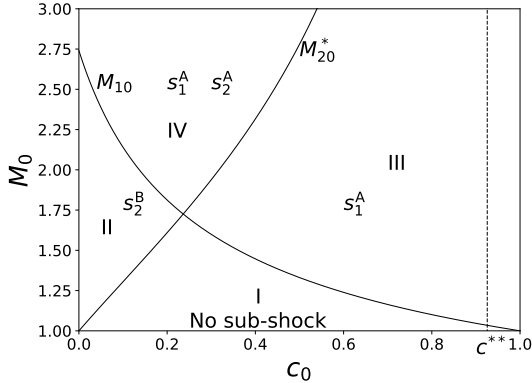


FIG. 1. Case A: Four regions in the plane (c_0, M_0) of possible sub-shocks in the case that M_{20}^* have a vertical asymptote in $c_0 = c_0^* < 1$. Values are $\gamma_1 = 7/5$, $\gamma_2 = 9/7$, and $\mu = 0.145 < \mu^*$.

Mach numbers is equivalent that $M_0 > M_{20}^*$ where M_{20}^* is solution of

$$M_{21}(M_{20}^*, c, \mu) = M_{20}^*, \quad (32)$$

where we have indicates with $M_{21} = \lambda_{21}/a_0$, the dimensionless characteristic velocity behind the shock. We have the following expression:

$$M_{21} = \frac{2(M_0^2 - 1)}{(\gamma_0 + 1)M_0} + \sqrt{\frac{\{2 + (\gamma_0 - 1)M_0^2\}\{1 + \gamma_0(2M_0^2 - 1)\}}{(\gamma_0 + 1)^2 M_0^2}} \frac{\gamma_2 m_0}{\gamma_0 m_2},$$

and we obtain the solution of (32) as follows:

$$M_{20}^* = \sqrt{\frac{2m_2\gamma_0 + m_0\gamma_2(\gamma_0 - 1)}{\gamma_0\{2m_0\gamma_2 - m_2(\gamma_0 - 1)\}}}. \quad (33)$$

From the definitions of the average mass and the global ratio of the specific heats (5), we have

$$\lim_{c_0 \rightarrow 0} M_{20}^* = 1. \quad (34)$$

The existence of real value of M_{20}^* require $2m_0\gamma_2 - m_2(\gamma_0 - 1) > 0$, which implies

$$c_0 < c_0^* = \frac{\mu}{(\gamma_1 - 1)(\gamma_2 - 1)(1 - \mu)^2} \times \left(-1 + \mu + \gamma_1(1 - \mu) - \gamma_2(\gamma_1 - \gamma_2) + \sqrt{\Gamma} \right),$$

where $\Gamma = \gamma_2\{(\gamma_2 - 1)[2\gamma_1(\gamma_1 - 1) + \gamma_2 - 2\gamma_1\gamma_2 + \gamma_2^2] - 2\mu\gamma_1(\gamma_1 - 1)(\gamma_2 - 1) + \mu^2\gamma_2(\gamma_1 - 1)^2\}$. Let

$$\mu^* = \frac{\gamma_1 - 1}{2\gamma_2} \quad (35)$$

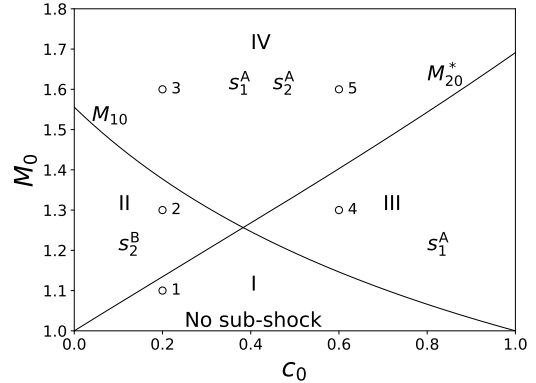


FIG. 2. Case A: Four regions in the plane (c_0, M_0) with $c_0^* > 1$ classified by the possibility of the sub-shock formation. The values are $\gamma_1 = 7/5$, $\gamma_2 = 9/7$, and $\mu = 0.45 > \mu^*$.

and we need to distinguish two cases: if $\mu < \mu^*$ then $c_0^* < 1$ and we have the Figure 1, while if $\mu > \mu^*$ then $c_0^* > 1$ and we show a typical example of the case for $\mu = 0.45$, $\gamma_1 = 7/5$, and $\gamma_2 = 9/7$ in Figure 2.

In both Figures 1 and 2, we have 4 regions in the plane (c_0, M_0) : in Region I, no sub-shock can exist, and the shock structure is always regular. In Region II, we may have a sub-shock for the variables of the second constituent S_2^B , where B represents before the maximum eigenvalue. In Region III, a sub-shock S_1^A for constituent 1 after the maximum characteristic velocity is predicted according to the theorem⁶. Finally, in Region IV, we have by sure the sub-shock S_1^A but may also have a sub-shock S_2^A ; in other words, in this region, we may have multiple sub-shocks. We summarize Case A as a statement:

Statement 1 - If the species with the smallest mass has fewer or equal degrees of freedom than the heavier one, we have for each value of the concentration the inequality (31) and the possible regions in the plane (c_0, M_0) where there may be sub-shocks are those described in Figure 1 and Figure 2. The curve $M_{20}^*(c_0)$ has a vertical asymptote in $c_0 = c_0^*$ for values of the ratio of the masses $\mu < \mu^*$ (Figure 1) and this implies that multiple sub-shocks can exists only for $c_0 < c_0^*$ while for $\mu > \mu^*$ there is no asymptote (Figure 2) and the multiple sub-shocks may exist for any value of concentration.

For completeness of the classification, we remark that there exists, at least mathematically, a very special case with $\mu = g = 1$. In this case, the characteristic velocities in equilibrium for both species (28) and also the characteristic velocity for the equilibrium subsystem (29) have the same value. Therefore $M_{10} = M_{20}^* = 1$ hold and there exists only Region IV. According to the theorem⁶, we conclude that no continuous solution exists and multiple sub-shocks connecting the unperturbed and perturbed states always appear for any $M_0 > 1$.

B. Case B: $\gamma_1 < \gamma_2$

Qualitatively different behavior is predicted when the degrees of freedom of lighter species is greater than the one of the heavy species because the topology of the regions changes with respect to Case A. In fact, we need to distinguish three cases as we increase the value of μ .

1. Case B₁: $\mu < g$

In this case we have as in Case A

$$\lambda_{20} < \lambda_{10}, \quad (36)$$

but the value of $\bar{\lambda}_0$ depends on the concentration. In fact, there exists a value of concentration \hat{c}_0 for which

$$\text{If } 0 < c_0 < \hat{c}_0, \quad \bar{\lambda}_0 < \lambda_{20} < \lambda_{10}, \quad s > \bar{\lambda}_0, \quad (37)$$

$$\text{If } \hat{c}_0 < c_0 < 1, \quad \lambda_{20} < \bar{\lambda}_0 < \lambda_{10}, \quad s > \bar{\lambda}_0. \quad (38)$$

In the first case (37) a new curve $M_{20}(c_0) > 1$ may emerge,

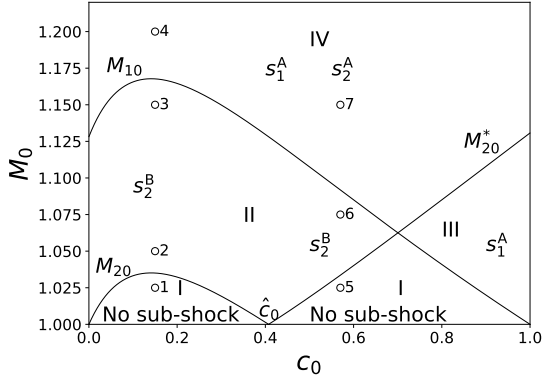


FIG. 3. Case B₁: Four regions in the plane (c_0, M_0) of possible sub-shocks. $\gamma_1 = 7/6$, $\gamma_2 = 5/3$, and $\mu = 0.55 < g$.

and a sub-shock S_2^B can exist if $M_{20} < M_0 < M_{10}$ with M_{20} being the dimensionless characteristic velocity of species 2:

$$M_{20} = \frac{\lambda_{20}}{a_0} = \sqrt{\frac{m_0 \gamma_2}{m_2 \gamma_0}} = \sqrt{\frac{\gamma_2 \mu}{\gamma_0 \{c_0 + (1 - c_0)\mu\}}}.$$

By solving $M_{20} \geq 1$, we obtain

$$0 < c_0 < \hat{c}_0 = \frac{\mu \{ \gamma_1 \gamma_2 (2 - \mu) - \gamma_1 - \gamma_2 (\gamma_2 - \mu) \}}{(1 - \mu) \{ \gamma_1 - \gamma_1 \gamma_2 (1 - \mu) - \gamma_2 \mu \}}. \quad (39)$$

It is simple to verify that $\hat{c}_0 < 1$ as $\mu < g$.

For value of concentration $c_0 > \hat{c}_0$ we have the inequalities (38) similar to the case A and we have the curve $M_{20}^*(c_0)$ given by (33). It is easy to verify that $M_{20}^*(\hat{c}_0) = 1$. An example with $\gamma_1 = 7/6$ and $\gamma_2 = 5/3$ and $\mu = 0.55$ is shown in Figure 3.

Although the topology of the regions is different from the one in Case A, we have the four regions I, II, III, and IV with

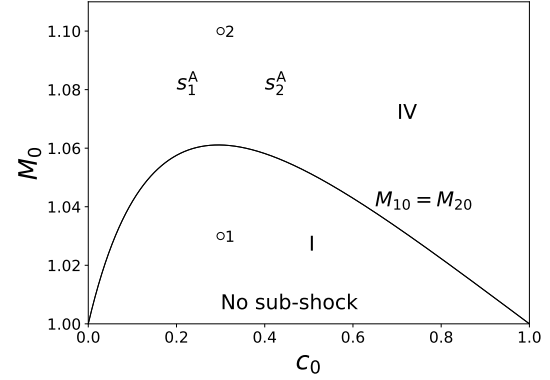


FIG. 4. Case B₂: Two regions in the plane (c_0, M_0) of possible sub-shocks. $\gamma_1 = 7/6$, $\gamma_2 = 5/3$, and $\mu = g = 0.7$.

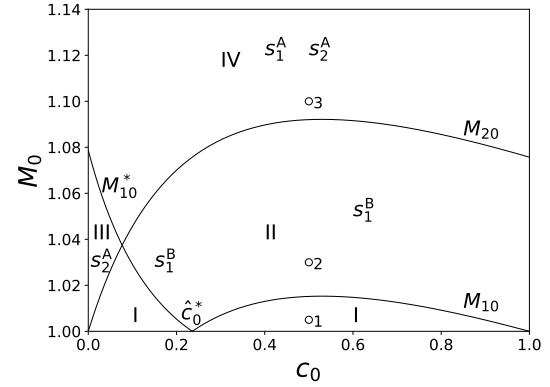


FIG. 5. Case B₃ - Four regions in the plane (c_0, M_0) of possible sub-shocks. $\gamma_1 = 7/6$, $\gamma_2 = 5/3$, and $\mu = 0.81 < \mu^{**}$.

the same possible sub-shocks that the one described in Case A: in Region I, no sub-shock emerges, in Region II, possible sub-shock in the species 2 may be formed, in Region III, sub-shock of species 1 appears, and in Region IV, both species can have sub-shocks.

2. Case B₂: $\mu = g$

When $\mu = g$, i.e. $m_1/m_2 = \gamma_1/\gamma_2$, we have the special situation in which the characteristic velocities of the two species in equilibrium are equal and $\hat{c}_0 = 1$ then (37) becomes:

$$\bar{\lambda}_0 < \lambda_{20} = \lambda_{10}, \quad s > \bar{\lambda}_0, \quad (40)$$

and as consequence $M_{20} = M_{10}$. We show this special case in Figure 4 by adopting $\mu = 0.7$, $\gamma_1 = 7/6$ and $\gamma_2 = 5/3$. This is an exceptional case where the regions become only two: regions I have no sub-shocks and region IV in which multiple sub-shock arise.

3. Case B_3 : $\mu > g$

Now the inequality (36) becomes opposite and the characteristic velocity of species 1 becomes greater than the one of the species 2:

$$\lambda_{10} < \lambda_{20}, \quad (41)$$

A sub-shock after the maximum characteristic velocity is observed when

$$s > \lambda_{20}$$

$$\Leftrightarrow M_0 > M_{20} = \frac{\lambda_{20}}{a_0} = \sqrt{\frac{m_0 \gamma_2}{m_2 \gamma_0}} = \sqrt{\frac{\gamma_2 \mu}{\gamma_0 \{c_0 + (1 - c_0) \mu\}}}.$$

It can be verified that

$$\lim_{c_0 \rightarrow 0} M_{20} = 1, \quad \lim_{c_0 \rightarrow 1} M_{20} = \sqrt{\frac{\mu}{g}}.$$

Now we have a specular situation as the case B_1 . There exists a value of the concentration \hat{c}_0^* such that

$$\text{If } 0 < c_0 < \hat{c}_0^*, \quad \lambda_{10} < \bar{\lambda}_0 < \lambda_{20}, \quad s > \bar{\lambda}_0, \quad (42)$$

$$\text{If } \hat{c}_0^* < c_0 < 1, \quad \bar{\lambda}_0 < \lambda_{10} < \lambda_{20}, \quad s > \bar{\lambda}_0. \quad (43)$$

In the case (42) we have the possibility that $\lambda_{II} = s$ and as consequence the curve $M_{II}(c_0)$ exist solution of

$$M_{II}(M_{10}^*, c, \mu) = M_{10}^*. \quad (44)$$

where we have indicates with $M_{II} = \lambda_{II}/a_0$, the dimensionless characteristic velocity in the equilibrium state behind the shock. We have the following expression of M_{II} :

$$M_{II} = \frac{2(M_0^2 - 1)}{(\gamma_0 + 1)M_0} + \sqrt{\frac{\{2 + (\gamma_0 - 1)M_0^2\}\{1 + \gamma_0(2M_0^2 - 1)\}}{(\gamma_0 + 1)^2 M_0^2} \frac{\gamma_1 m_0}{\gamma_0 m_1}},$$

and in this case the solution of (44) is given by

$$M_{10}^* = \sqrt{\frac{2m_1 \gamma_0 + m_0 \gamma_1 (\gamma_0 - 1)}{\gamma_0 \{2m_0 \gamma_1 - m_1 (\gamma_0 - 1)\}}}.$$

It is easy to verify that M_{10}^* is always a real number and is greater or equal to 1 if $0 < c_0 \leq \hat{c}_0^*$ with

$$\hat{c}_0^* = \frac{\mu(\gamma_1 - 1)(\gamma_1 - \gamma_2 \mu)}{(1 - \mu)\{\gamma_1 - \gamma_1 \gamma_2 (1 - \mu) - \gamma_2 \mu\}}. \quad (45)$$

Moreover

$$\lim_{c_0 \rightarrow 0} M_{10}^* = \sqrt{\frac{\gamma_1(\gamma_2 - 1) + 2\gamma_2 \mu}{\gamma_2 \{2\gamma_1 - \mu(\gamma_2 - 1)\}}}, \quad \lim_{c_0 \rightarrow \hat{c}_0^*} M_{10}^* = 1.$$

It is easy to verify that $\hat{c}_0^* < 1$ if $\mu < \mu^{**}$ with

$$\mu^{**} = \frac{\gamma_1(1 - \gamma_2)}{\gamma_1^2 + \gamma_2 - 2\gamma_1 \gamma_2}. \quad (46)$$

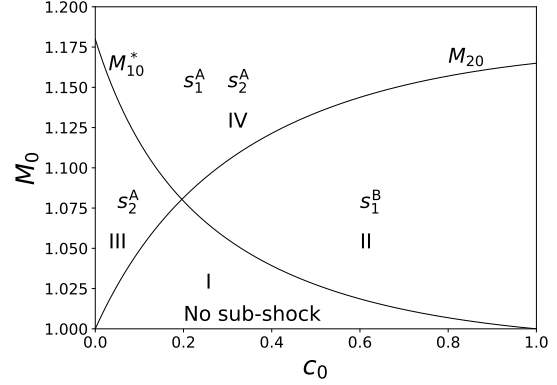


FIG. 6. Case B_3 - Four regions in the plane (c_0, M_0) of possible sub-shocks in a binary Eulerian mixture. $\gamma_1 = 7/6$, $\gamma_2 = 5/3$, and $\mu = 0.95 > \mu^{**}$.

Then if $\mu < \mu^{**}$ and $c_0 > \hat{c}_0^*$ we have the inequalities (43) and in this case emerges the curve $M_{10} \geq 1$

$$M_{10} = \frac{\lambda_{10}}{a_0} = \sqrt{\frac{m_0 \gamma_1}{m_1 \gamma_0}} = \sqrt{\frac{\gamma_1}{\gamma_0 \{c_0 + (1 - c_0) \mu\}}},$$

with the property that $M_{10} = 1$ when $c_0 = \hat{c}_0^*$ and $c_0 = 1$.

As a typical example, we depict the curves with $\mu = 0.81$, $\gamma_1 = 7/6$, $\gamma_2 = 5/3$ in Figure 5.

While if $\mu > \mu^{**}$ we have $\hat{c}_0 > 1$ and only the case (42) hold and we have only the curve M_{10}^* in all the interval of concentration. As a typical example, we depict the curves with $\mu = 0.95$, $\gamma_1 = 7/6$, and $\gamma_2 = 5/3$ in Figure 6.

In Case B_3 we have: in Region I, shock structure is always continuous, in Region II, there may exist a sub-shock for the variables of first species S_1^B , in Region III, we have a sub-shock S_2^A for constituent 2 and finally, in Region IV, we may have multiple sub-shocks for both constituent S_1^A, S_2^A after the maximum eigenvalue in the unperturbed state. Summarizing the case B as a statement:

Statement 2 - If the species with the smallest mass has more degrees of freedom than the heavier one, we have a different topology of the regions for increasing values of the ratio of masses μ . For $0 < \mu < g$, the regions are the ones described in Figure 3, and the characteristic velocity of heavy species is less than the one with smallest mass (36). For $\mu = g$, the characteristic velocity of both species are equal, and the possible regions reduce only to two as in Figure 4. Then for $\mu > g$ we have the inversion between the two characteristic velocities (41) and we have the Figures 5 and 6 respectively for $\mu < \mu^{**}$ and for $\mu > \mu^{**}$ with μ^{**} given by (46).

V. NUMERICAL RESULTS ON THE SHOCK STRUCTURE

In the previous section, from the possibility for the sub-shock formation, we have identified regions for different values of the parameters in the plane (c_0, M_0) . However, we

are sure that sub-shocks exist only when the shock velocity is greater than the maximum characteristic velocities evaluated in the equilibrium state in front of the shock by the Boillat and Ruggeri theorem⁶, or we are sure in Region I that we have a regular structure without sub-shock formation. In the other case, we have only a necessary condition for the existence of sub-shocks, and we do not know theoretically if these sub-shocks arise. We understand the reason why the condition $s = \lambda$ is not in general sufficient in the following way. If we multiply the system (18) by the left eigenvector \mathbf{l} of \mathbf{A} corresponding to a given eigenvalue λ , we obtain

$$\mathbf{l} \cdot \frac{d\mathbf{u}}{d\varphi} = \frac{\mathbf{l} \cdot \mathbf{P}}{\lambda - s}.$$

Therefore the shock structure can be regular if $\mathbf{l} \cdot \mathbf{P}$ should tend to zero as s approaches the eigenvalue λ . This is not an exceptional case because, at least in cases of a single fluid in the framework of RET studied in the literature^{3,7,8,11}, this is always present except for the maximum eigenvalue evaluated in equilibrium. Therefore we need to solve the system

of field equations numerically and make the possibility of the sub-shock formation clear in the different points of each region.

A. Dimensionless field equations and phenomenological coefficients

For convenience, we introduce the following dimensionless variables scaled by the values evaluated in the unperturbed state:

$$\begin{aligned} \hat{\rho} &= \frac{\rho}{\rho_0}, & \hat{v} &= \frac{v}{a_0}, & \hat{T} &= \frac{T}{T_0}, & \hat{x} &= \frac{x}{t_c a_0}, & \hat{t} &= \frac{t}{t_c}, \\ \hat{\psi} &= \frac{t_c}{\rho_0 T_0} \psi, & \hat{\theta} &= \frac{t_c}{\rho_0 \frac{k_B}{m_0} T_0^2} \theta, \end{aligned} \quad (47)$$

where t_c is arbitrary characteristic time for numerical computations. The system (8) is rewritten as

$$\begin{aligned} \frac{\partial \hat{\rho}_1}{\partial \hat{t}} + \frac{\partial \hat{\rho}_1 \hat{v}_1}{\partial \hat{x}} &= 0, \\ \frac{\partial \hat{\rho}_1 \hat{v}_1}{\partial \hat{t}} + \frac{\partial}{\partial \hat{x}} \left\{ \hat{\rho}_1 \left(\hat{v}_1^2 + \frac{\hat{T}_1}{\gamma_0 \{c + (1-c)\mu\}} \right) \right\} &= -\hat{\psi} \frac{(\hat{v}_1 - \hat{v}_2)(\hat{\rho}_1 \hat{T}_1 + \hat{\rho}_2 \hat{T}_2)}{(\hat{\rho}_1 + \hat{\rho}_2) \hat{T}_1 \hat{T}_2}, \\ \frac{\partial}{\partial \hat{t}} \left\{ \hat{\rho}_1 \left(\hat{v}_1^2 + \frac{2\hat{T}_1}{\gamma_0(\gamma_1-1) \{c + (1-c)\mu\}} \right) \right\} + \frac{\partial}{\partial \hat{x}} \left\{ \hat{\rho}_1 \hat{v}_1 \left(\hat{v}_1^2 + \frac{2\gamma_1 \hat{T}_1}{\gamma_0(\gamma_1-1) \{c + (1-c)\mu\}} \right) \right\} &= -2 \frac{\hat{\theta}}{\gamma_0} \frac{(\hat{T}_1 - \hat{T}_2)}{\hat{T}_1 \hat{T}_2} - 2\hat{\psi} \frac{(\hat{v}_1 - \hat{v}_2)(\hat{\rho}_1 \hat{v}_1 + \hat{\rho}_2 \hat{v}_2)(\hat{\rho}_1 \hat{T}_1 + \hat{\rho}_2 \hat{T}_2)}{(\hat{\rho}_1 + \hat{\rho}_2)^2 \hat{T}_1 \hat{T}_2}, \\ \frac{\partial \hat{\rho}_2}{\partial \hat{t}} + \frac{\partial \hat{\rho}_2 \hat{v}_2}{\partial \hat{x}} &= 0, \\ \frac{\partial \hat{\rho}_2 \hat{v}_2}{\partial \hat{t}} + \frac{\partial}{\partial \hat{x}} \left\{ \hat{\rho}_2 \left(\hat{v}_2^2 + \frac{\mu \hat{T}_2}{\gamma_0 \{c + (1-c)\mu\}} \right) \right\} &= \hat{\psi} \frac{(\hat{v}_1 - \hat{v}_2)(\hat{\rho}_1 \hat{T}_1 + \hat{\rho}_2 \hat{T}_2)}{(\hat{\rho}_1 + \hat{\rho}_2) \hat{T}_1 \hat{T}_2}, \\ \frac{\partial}{\partial \hat{t}} \left\{ \hat{\rho}_2 \left(\hat{v}_2^2 + \frac{2\mu \hat{T}_2}{\gamma_0(\gamma_2-1) \{c + (1-c)\mu\}} \right) \right\} + \frac{\partial}{\partial \hat{x}} \left\{ \hat{\rho}_2 \hat{v}_2 \left(\hat{v}_2^2 + \frac{2\gamma_2 \mu \hat{T}_2}{\gamma_0(\gamma_2-1) \{c + (1-c)\mu\}} \right) \right\} &= 2 \frac{\hat{\theta}}{\gamma_0} \frac{(\hat{T}_1 - \hat{T}_2)}{\hat{T}_1 \hat{T}_2} + 2\hat{\psi} \frac{(\hat{v}_1 - \hat{v}_2)(\hat{\rho}_1 \hat{v}_1 + \hat{\rho}_2 \hat{v}_2)(\hat{\rho}_1 \hat{T}_1 + \hat{\rho}_2 \hat{T}_2)}{(\hat{\rho}_1 + \hat{\rho}_2)^2 \hat{T}_1 \hat{T}_2}, \end{aligned} \quad (48)$$

Next we need to estimate the values of the dimensionless phenomenological coefficients $\hat{\psi}$ and $\hat{\theta}$ defined in (47). Both $\hat{\psi}$ and $\hat{\theta}$ are proportional to the characteristic time t_c and therefore only the ratio $\hat{\psi}/\hat{\theta}$ is important for the present analysis. There are at least two kinds of expressions from kinetic-theoretical considerations for rarefied monatomic/polyatomic gases^{25–27}. While the detailed expressions proposed of these two models are different from each other, the values of $\hat{\psi}$ and $\hat{\theta}$ seem the same order of magnitude. For discussing typical examples of the shock structure and the sub-shock formation, we adopt the following constant values of the phenomenological coefficients: $\hat{\psi} = \hat{\theta} = 0.1$.

B. Numerical methods

In the present analysis, in order to obtain the shock-structure solution with or without sub-shocks, we use a different procedure solving ad hoc Riemann problem for the PDE system (7) instead of solving the ODE system (18). This strategy is based on the conjecture about the large-time behavior of the Riemann problem and the Riemann problem with structure^{28,29} for a system of balance laws proposed by Ruggeri and coworkers^{30–32} – following an idea of Liu³³. According to this conjecture, the solutions of both Riemann problems with and without structure, for large time, instead of converg-

ing to the corresponding Riemann problem of the equilibrium subsystem (i.e combination of shock and rarefaction waves), converge to solutions that represent a combination of shock structures (with and without sub-shocks) of the full system and rarefaction waves of the equilibrium subsystem.

In particular, if the Riemann initial data correspond to a shock family \mathcal{S} of the equilibrium subsystem, for a large time, the solution of the Riemann problem of the full system converges to the corresponding shock structure. This strategy allows us to use the Riemann solvers³⁴ for numerical calculations of the shock structure and was adopted in several shock phenomena of RET¹⁰. In particular, the conjecture was tested numerically for a Grad 13-moment system and a mixture of fluids^{30,35} and was verified in a simple 2×2 dissipative models^{9,15,32}.

We perform numerical calculations on the shock structure obtained after a long time for the Riemann problem consisting of two equilibrium states \mathbf{u}_0 and \mathbf{u}_1 satisfying (24) and (25). The initial discontinuity between \mathbf{u}_0 and \mathbf{u}_1 is set to be located at $\hat{x} = 0$. We have developed numerical code written in Python on the basis of the Uniformly accurate Central Scheme of order 2 (UCS2) proposed by Liotta, Romano, and Russo³⁶ for analyzing the hyperbolic balance laws with production terms. As the UCS2 is an implicit scheme, we need to solve the derived nonlinear difference equations iteratively for every time step by using an appropriate library such as SciPy³⁷. We check the convergence of the asymptotic profile and the independence of the size of spatial mesh $\Delta\hat{x}$ and temporal mesh $\Delta\hat{t}$ carefully.

C. Shock structure in Case A

In this subsection, for discussing the sub-shock formation in Case A, we adopt the following parameters: $\gamma_1 = 7/5$, $\gamma_2 = 9/7$, and $\mu = 0.4$. In Figures 7 – 9, we show the profiles of the dimensionless mass density, the dimensionless velocity and the dimensionless temperature for several Mach numbers in the case of $c_0 = 0.2$. Figure 7 shows the shock structure for $M_0 = 1.1$, which corresponds to the parameter in Region I and, as expected, we confirm that the shock structure is continuous and no sub-shock appears.

Figure 8 shows the shock structure for $M_0 = 1.3$, which corresponds to a parameter in Region II in which the necessary condition of the sub-shock formation is satisfied, and we see that very steep change of the physical quantities of constituent 2. In order to distinguish a real sub-shock from a continuous part with a very steep gradient, we adopt a method proposed in a paper on the shock structure in a binary mixture of monatomic gases¹², which uses the fact that the jump of a sub-shock must satisfy the compatibility conditions, namely, the Rankine-Hugoniot (RH) conditions for the full system. For the full system (48), we have the following expression of the

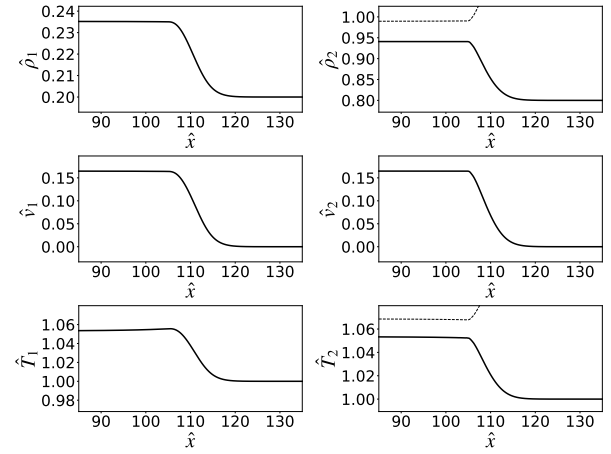


FIG. 7. Case A: Profiles of the dimensionless mass density, velocity and temperature for the constituent 1 of light molecules (left) and for the constituent 2 of heavy molecules (right) at $\hat{t} = 100$. The parameters are set to be in Region I and correspond to No. 1 in Figure 2 of Case A1; $\gamma_1 = 7/5$, $\gamma_2 = 9/7$, $\mu = 0.45$, $c_0 = 0.2$, and $M_0 = 1.1$. The temporal and spatial numerical meshes are $\Delta\hat{t} = 0.025$ and $\Delta\hat{x} = 0.1$.

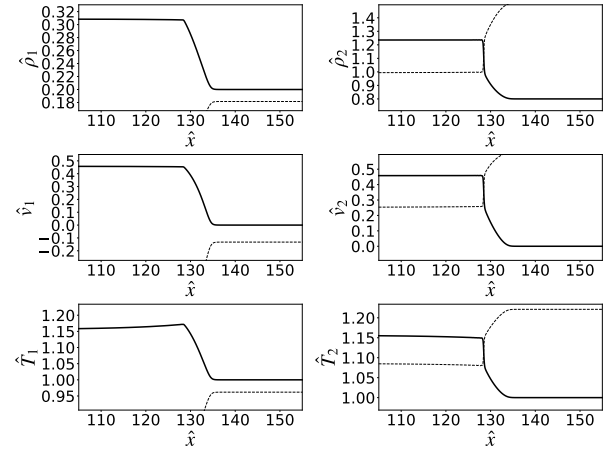


FIG. 8. Case A: Shock structure in a binary Eulerian mixture of polyatomic gases obtained at $\hat{t} = 100$ (Solid curves). The parameters are in Region II and correspond to the mark of No. 2 shown in Figure 2; $\gamma_1 = 7/5$, $\gamma_2 = 9/7$, $\mu = 0.45$, $c_0 = 0.2$, and $M_0 = 1.3$. The numerical conditions are $\Delta\hat{t} = 0.01$ and $\Delta\hat{x} = 0.08$. The curves of the potential sub-shock predicted any point of the shock structure are also shown (dotted curves).

state just after the sub-shock:

$$\begin{aligned}
 \rho_1^* &= \frac{(\gamma_1 + 1)M_1^2}{2 + (\gamma_1 - 1)M_1^2} \hat{\rho}_1, \\
 \hat{v}_1^* &= \hat{v}_1 + \frac{2(M_1^2 - 1)}{(\gamma_1 + 1)M_1} \frac{a_1}{a_0}, \\
 \hat{T}_1^* &= \frac{\{2 + (\gamma_1 - 1)M_1^2\} \{1 + \gamma_1(2M_1^2 - 1)\}}{(\gamma_1 + 1)^2 M_1^2} \hat{T}_1, \\
 \rho_2^* &= \frac{(\gamma_2 + 1)M_2^2}{2 + (\gamma_2 - 1)M_2^2} \hat{\rho}_2, \\
 \hat{v}_2^* &= \hat{v}_2 + \frac{2(M_2^2 - 1)}{(\gamma_2 + 1)M_2} \frac{a_2}{a_0}, \\
 \hat{T}_2^* &= \frac{\{2 + (\gamma_2 - 1)M_2^2\} \{1 + \gamma_2(2M_2^2 - 1)\}}{(\gamma_2 + 1)^2 M_2^2} \hat{T}_2,
 \end{aligned} \tag{49}$$

where the quantities with superscript * represent the quantities in the state just after a sub-shock predicted by the RH condition of the full system. Here M_1 and M_2 are the Mach numbers for the constituent 1 and 2:

$$M_1 \equiv \frac{s - v_1}{a_1} = (M_0 - \hat{v}_1) \frac{a_0}{a_1}, \quad M_2 \equiv \frac{s - v_2}{a_2} = (M_0 - \hat{v}_2) \frac{a_0}{a_2},$$

where a_1 and a_2 are the sound velocity for the constituent 1 and 2, respectively and the following relations hold:

$$\frac{a_0}{a_1} = \sqrt{\frac{\gamma_0}{\gamma_1 \hat{T}_1} \{c + (1-c)\mu\}}, \quad \frac{a_0}{a_2} = \sqrt{\frac{\gamma_0}{\gamma_2 \hat{T}_2} \left\{ \frac{c}{\mu} + (1-c) \right\}}.$$

In all figures for the shock structure, we depict the profile of the physical quantities with the curve representing potential state just after the sub-shock predicted by (49) from any point of the shock structure. Although a sub-shock is captured with a very steep but continuous change in numerical calculations due to the numerical viscosity, it can be expected that the part of a sub-shock is approximately described as a part joining the curve of the potential sub-shock. Therefore the curve representing potential sub-shock can be regarded as a useful indicator of the behavior of the shock-structure solution.

By drawing two curves together, from Figure 8, we see that a sub-shock appears in the profile of the constituent 2 for $M_0 = 1.3$. As discussed in the previous section, in the present case in Region II, the shock velocity for the Mach number $M_0 = 1.3$ is slower than the maximum characteristic velocity evaluated in the unperturbed state. Therefore, we conclude that there exists a clear counter-example of the conjecture on the sub-shock formation also in the case of a mixture of rarefied polyatomic gases.

We show the shock structure for $M_0 = 1.6$ in Figure 9 and understand that sub-shocks are observed in both the profiles for constituents 1 and 2. It is concluded that multiple sub-shocks are predicted with the parameters in Region IV.

The shock structure for several Mach numbers with $c_0 = 0.6$ is shown in figures 10 and 11. We understand that a sub-shock is formed for the constituent 1 for $M_0 = 1.3$ in Region III from Figure 10. From Figure 11 showing the case for

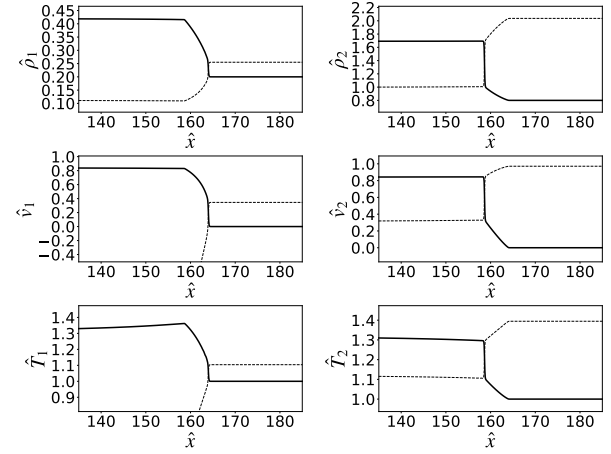


FIG. 9. Case A: Shock structure in a binary Eulerian mixture of polyatomic gases obtained at $\hat{t} = 100$. The parameters are in Region IV and correspond to the mark of No. 3 shown in Figure 2; $\gamma_1 = 7/5$, $\gamma_2 = 9/7$, $\mu = 0.45$, $c_0 = 0.2$, and $M_0 = 1.6$. The numerical conditions are $\Delta\hat{t} = 0.01$ and $\Delta\hat{x} = 0.08$.

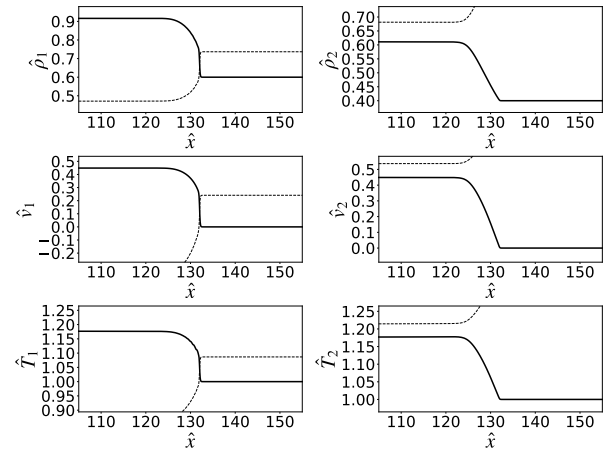


FIG. 10. Case A: Shock structure in a binary Eulerian mixture of polyatomic gases obtained at $\hat{t} = 100$. The parameters are in Region III and correspond to the mark of No. 4 shown in Figure 2; $\gamma_1 = 7/5$, $\gamma_2 = 9/7$, $\mu = 0.45$, $c_0 = 0.6$, and $M_0 = 1.3$. The numerical conditions are $\hat{t} = 0.01$ and $\hat{x} = 0.08$.

$M_0 = 1.6$ in region IV, we see that multiple sub-shocks for both species 1 and 2 appear.

To summarize the results obtained in the case of $\mu = 0.45$, $\gamma_1 = 7/5$, $\gamma_2 = 9/7$, from the viewpoint of the sub-shock formation, the predictions are similar to the ones observed in the context of the shock structure in a mixture of rarefied monatomic gases. Counter-example of the conjecture on the sub-shock formation can be constructed with the parameters in Region II, and multiple sub-shocks are also observed with the parameters in Region IV.

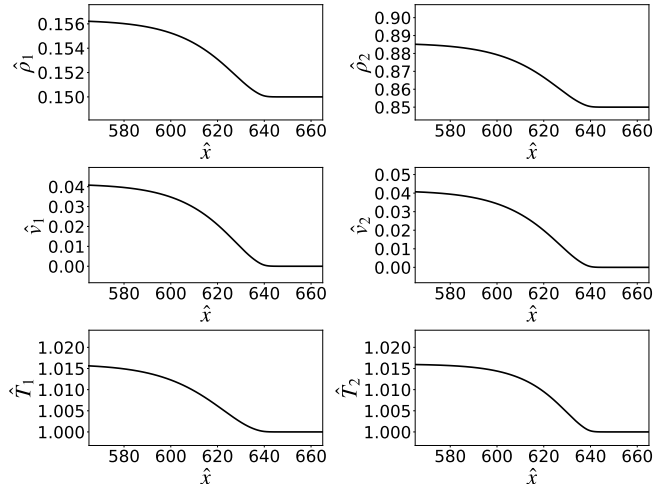
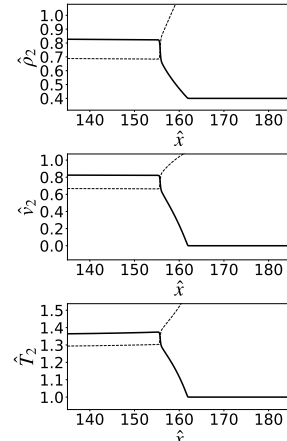
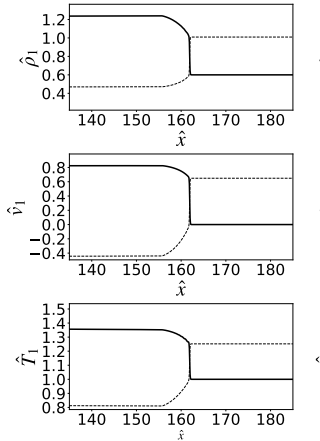


FIG. 11. Case A: Shock structure in a binary Eulerian mixture of polyatomic gases obtained at $\hat{t} = 100$. The parameters are in Region IV and correspond to the mark of No. 5 shown in Figure 2; $\gamma_1 = 7/5$, $\gamma_2 = 9/7$, $\mu = 0.45$, $c_0 = 0.6$, and $M_0 = 1.6$. The numerical conditions are $\Delta\hat{t} = 0.01$ and $\Delta\hat{x} = 0.08$.

D. Shock structure in Case B₁

Next let us analyze the shock structure with $\mu = 0.55$, $\gamma_1 = 7/6$, and $\gamma_2 = 5/3$ for different concentrations and the Mach numbers. In the case of $c_0 = 0.15$, we show the shock structure for $M_0 = 1.025, 1.05, 1.15$, and 1.2 in Figures 12 – 15. Figure 13 for $M_0 = 1.05$ shows a surprising result that a sub-shock for constituent 1 does not emerge even with $M_0 > M_{20}$. Although the curves of the potential sub-shock are intersected by the profile of the physical quantities, the shock structure is continuous and no sub-shock appears.

Let us consider the behavior of $\mathbf{l} \cdot \mathbf{P}$ in the shock-structure solution for the constituent 2, and we focus on the mode corresponding to λ_2 . The left eigenvector \mathbf{l}_2 for the system (7) corresponding to λ_2 is

$$\mathbf{l}_2 = \begin{bmatrix} 0 \\ 0 \\ 0 \\ v_2 \left(v_2 - \sqrt{\gamma_2 \frac{k_B}{m_2} T_2} \right) \\ \sqrt{\gamma_2 \frac{k_B}{m_2} T_2} - 2v_2 \\ 1 \end{bmatrix}^T$$

and we depict its profile in the dimensionless form given by $t_c \mathbf{l}_2 \cdot \mathbf{P} / (\rho_0 a_0^2)$ in Figure 13. From Figure 13, it is confirmed that $\mathbf{l}_2 \cdot \mathbf{P}$ becomes zero at the intersection point between the profile and the curve of the potential sub-shock. Therefore we conclude that the shock structure for constituent 2 is continuous without any sub-shock.

The shock structure for $M_0 = 1.15$ is shown in Figure 14, which lies in the same region in the case with $M_0 = 1.05$ in Figure 3. Again surprisingly, from Figure 14, we see a sub-shock for constituent 2 emerges for $M_0 = 1.15$. We conclude that the regular singular point corresponding to the second-fastest mode for constituent 2 observed for $M_0 = 1.15$ is no

FIG. 12. Case B₁: Shock structure in a binary Eulerian mixture of polyatomic and monatomic gases obtained at $\hat{t} = 600$. The parameters are in Region I and correspond to the mark of No. 1 shown in Figure 3; $\gamma_1 = 7/6$, $\gamma_2 = 5/3$, $\mu = 0.55$, $c_0 = 0.15$, and $M_0 = 1.025$. The numerical conditions are $\Delta\hat{x} = 0.02$ and $\Delta\hat{t} = 0.08$.

more regular, and a sub-shock also for constituent 2 emerges. This is also the first example that a singular point is a regular singular for the moderately large Mach number, and this regular singular point becomes singular for the larger Mach number.

The fact that singular points in the shock-structure solution become regular is similar to the ones reported in the context of single fluids of rarefied monatomic and polyatomic gases^{8,9}. The singular point becoming regular is called a *regular singular point*. Nevertheless, to the authors' knowledge, the present result is the first example in which the singular point of the shock-structure solution becomes a regular singular point in the context of mixtures of rarefied gases.

In the case of $c_0 = 0.57$, we show the shock structure for $M_0 = 1.025, 1.075, 1.15$ in Figures 16 – 18. We confirm the similar behavior that continuous shock structure for $M_0 = 1.025$ becomes the shock structure with a regular singular point for $M_0 = 1.075$ and then the multiple sub-shocks appear for $M_0 = 1.15$.

In summary, in the present case, we understand that the singular point may become regular for the moderately large Mach number. However, the corresponding singular point may become singular for the larger Mach number even with the same production terms. Therefore it is impossible to conclude the possibility of the sub-shock formation a priori even if we write down the production terms explicitly. The numerical analysis of the shock-structure solution is necessary to conclude whether the sub-shock forms or not if we adopt the parameters.

By performing many numerical calculations of the shock structure, in principle, we obtain the boundary between the regular singular and singular points. For classification of the regions in more detail, the method of dynamical analysis of the ODE system is also useful. Please see Appendix A for

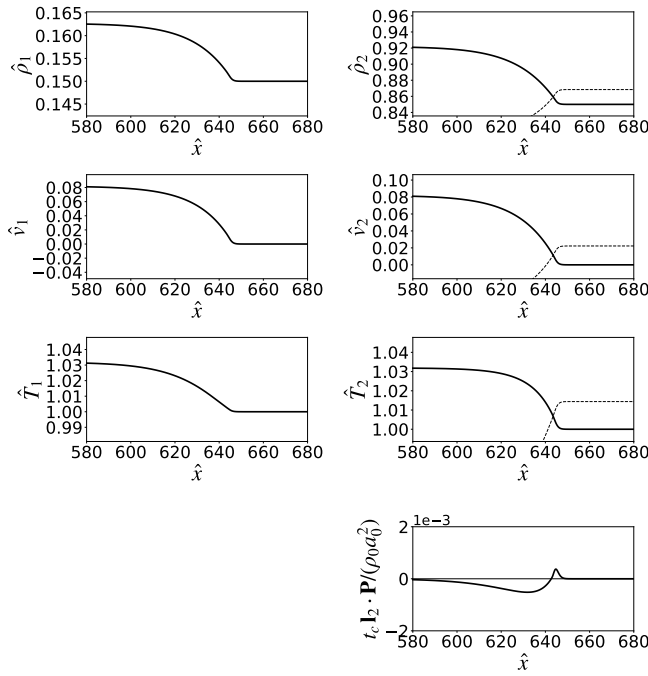


FIG. 13. Case B₁: Shock structure in a binary Eulerian mixture of polyatomic and monatomic gases obtained at $\hat{t} = 600$. The parameters are in Region II and correspond to the mark of No. 2 shown in Figure 3; $\gamma_1 = 7/6$, $\gamma_2 = 5/3$, $\mu = 0.55$, $c_0 = 0.15$, and $M_0 = 1.05$. The numerical conditions are $\Delta\hat{t} = 0.02$ and $\Delta\hat{x} = 0.08$. The profiles of the potential sub-shock predicted by the RH conditions of the full system are also shown (dotted curves).

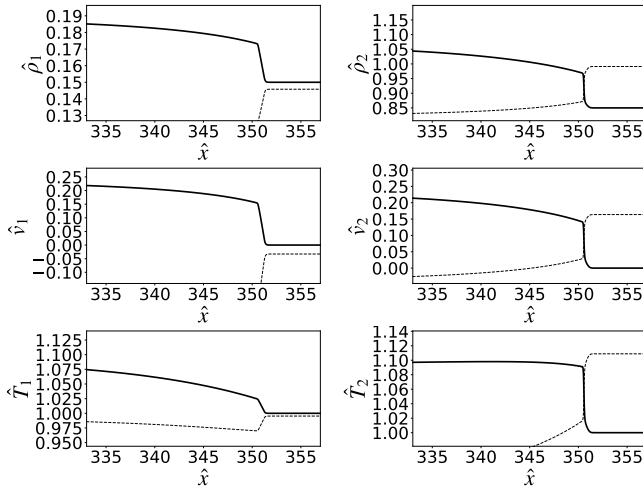


FIG. 14. Case B₁: Shock structure in a binary Eulerian mixture of polyatomic and monatomic gases obtained at $\hat{t} = 300$. The parameters are in Region II and correspond to the mark of No. 3 shown in Figure 3; $\gamma_1 = 7/6$, $\gamma_2 = 5/3$, $\mu = 0.55$, $c_0 = 0.15$, and $M_0 = 1.15$. The numerical conditions are $\Delta\hat{t} = 0.01$ and $\Delta\hat{x} = 0.04$.

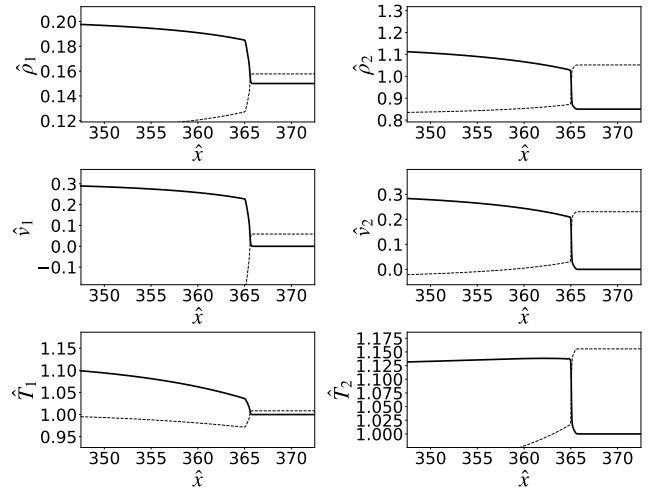


FIG. 15. Case B₁: Shock structure in a binary Eulerian mixture of polyatomic and monatomic gases obtained at $\hat{t} = 300$. The parameters are in Region IV and correspond to the mark of No. 4 shown in Figure 3; $\gamma_1 = 7/6$, $\gamma_2 = 5/3$, $\mu = 0.55$, $c_0 = 0.15$, and $M_0 = 1.2$. The numerical conditions are $\Delta\hat{t} = 0.01$ and $\Delta\hat{x} = 0.04$.

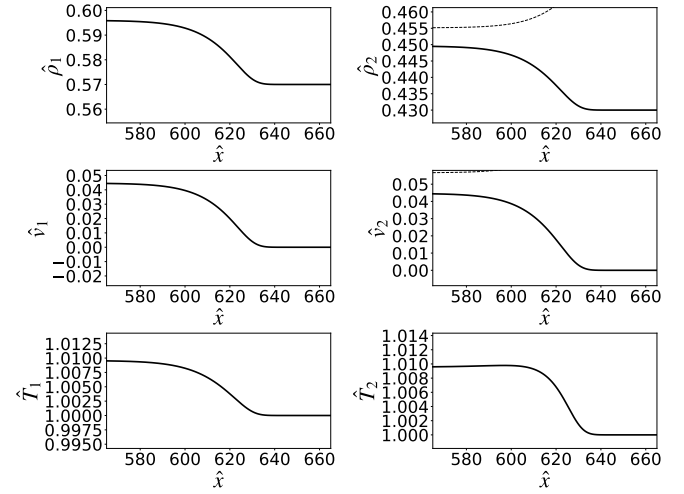


FIG. 16. Case B₁: Shock structure in a binary Eulerian mixture of polyatomic and monatomic gases obtained at $\hat{t} = 600$. The parameters are in Region I and correspond to the mark of No. 5 shown in Figure 3; $\gamma_1 = 7/6$, $\gamma_2 = 5/3$, $\mu = 0.55$, $c_0 = 0.57$, and $M_0 = 1.025$. The numerical conditions are $\Delta\hat{t} = 0.02$ and $\Delta\hat{x} = 0.08$.

detail of the method.

E. Shock structure in Case B₂

We show the shock structure with $\gamma_1 = 7/6$, $\gamma_2 = 5/3$, $\mu = 0.7$, and $c_0 = 0.3$ for $M_0 = 1.03$ in Figure 19 and for $M_0 = 1.1$ in Figure 20. As is expected, we observe a continuous shock structure for $M_0 = 1.03$ corresponding to the parameters in Region I and a shock structure with multiple sub-

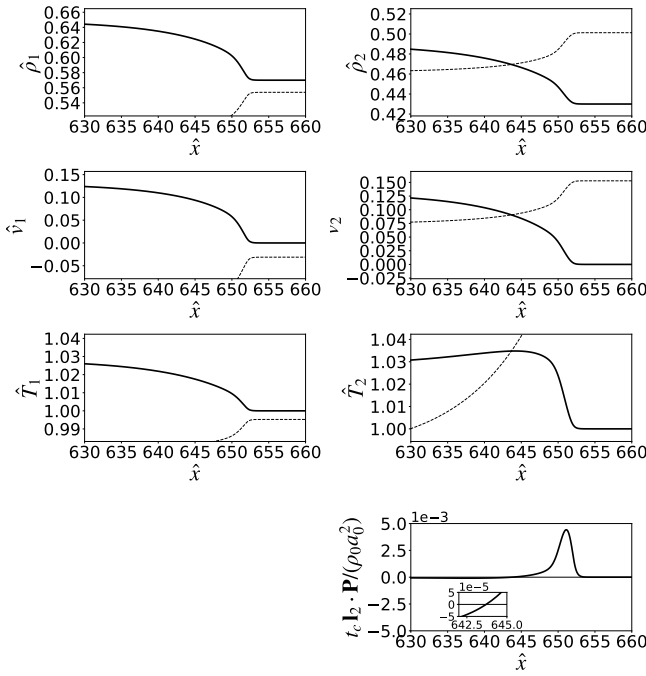


FIG. 17. Case B₁: Shock structure in a binary Eulerian mixture of polyatomic and monatomic gases obtained at $\hat{t} = 600$. The parameters are in Region II and correspond to the mark of No. 6 shown in Figure 3; $\gamma_1 = 7/6$, $\gamma_2 = 5/3$, $\mu = 0.55$, $c_0 = 0.57$, and $M_0 = 1.075$. The numerical conditions are $\Delta\hat{t} = 0.02$ and $\Delta\hat{x} = 0.08$.

shocks for $M_0 = 1.1$ corresponding to the parameters in Region IV. It is noticeable that both sub-shocks for constituents 1 and 2 arise from the unperturbed state in contrast to other examples of the multiple sub-shock formation. Because both characteristic velocities in the unperturbed state have the common maximum value in this special case, both sub-shocks should be connected with the unperturbed state according to the theorem⁶.

F. Shock structure in Case B₃

In this subsection, in order to discuss the sub-shock formation in Case B₃, we adopt the following parameters; $\gamma_1 = 7/6$, $\gamma_2 = 5/3$ and $\mu = 0.81$. Figures 21 – 23 show the shock structure for several Mach numbers in the case of $c_0 = 0.5$. We confirm from Figure 21 that the shock structure for $M_0 = 1.005$ is continuous and no sub-shock appears as expected.

Again no sub-shock emerges in the shock structure for $M_0 = 1.03$ shown in Figure 22 although the shock velocity is greater than the characteristic velocity for the species 1 evaluated in the unperturbed state. The left eigenvector \mathbf{I}_1 for the

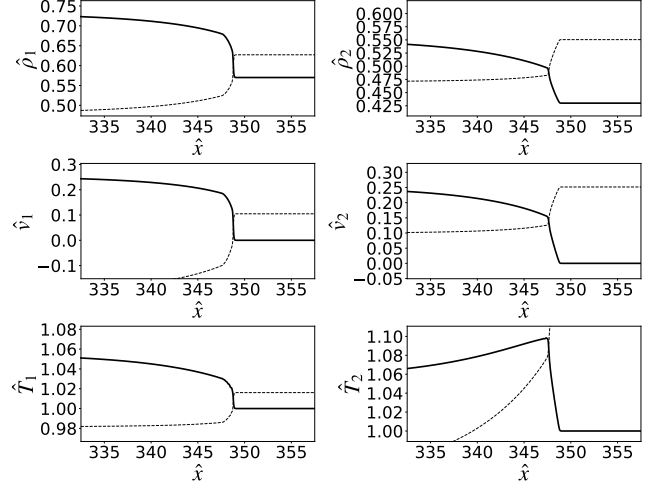


FIG. 18. Case B₁: Shock structure in a binary Eulerian mixture of polyatomic and monatomic gases obtained at $\hat{t} = 300$. The parameters are in Region IV and correspond to the mark of No. 7 shown in Figure 3; $\gamma_1 = 7/6$, $\gamma_2 = 5/3$, $\mu = 0.55$, $c_0 = 0.57$, and $M_0 = 1.15$. The numerical conditions are $\Delta\hat{t} = 0.01$ and $\Delta\hat{x} = 0.04$.

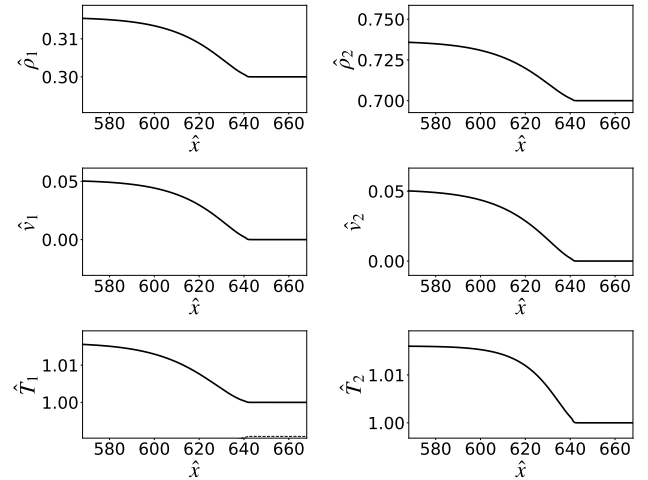


FIG. 19. Case B₂: Shock structure in a binary Eulerian mixture of polyatomic and monatomic gases obtained at $\hat{t} = 600$. The parameters are in Region I and correspond to the mark of No. 1 shown in Figure 4; $\gamma_1 = 7/6$, $\gamma_2 = 5/3$, $\mu = 0.7$, $c_0 = 0.3$, and $M_0 = 1.03$. The numerical conditions are $\Delta\hat{t} = 0.02$ and $\Delta\hat{x} = 0.08$.

system (7) corresponding to λ_1 is

$$\mathbf{I}_1 = \begin{bmatrix} v_1 \left(v_1 - \sqrt{\gamma_1 \frac{k_B}{m_1} T_1} \right) \\ \sqrt{\gamma_1 \frac{k_B}{m_1} T_1} - 2v_1 \\ 1 \\ 0 \\ 0 \\ 0 \end{bmatrix}^T$$

From the profile of the $t_c \mathbf{I}_1 \cdot \mathbf{P} / (\rho_0 a_0^2)$ shown in Figure 22 we

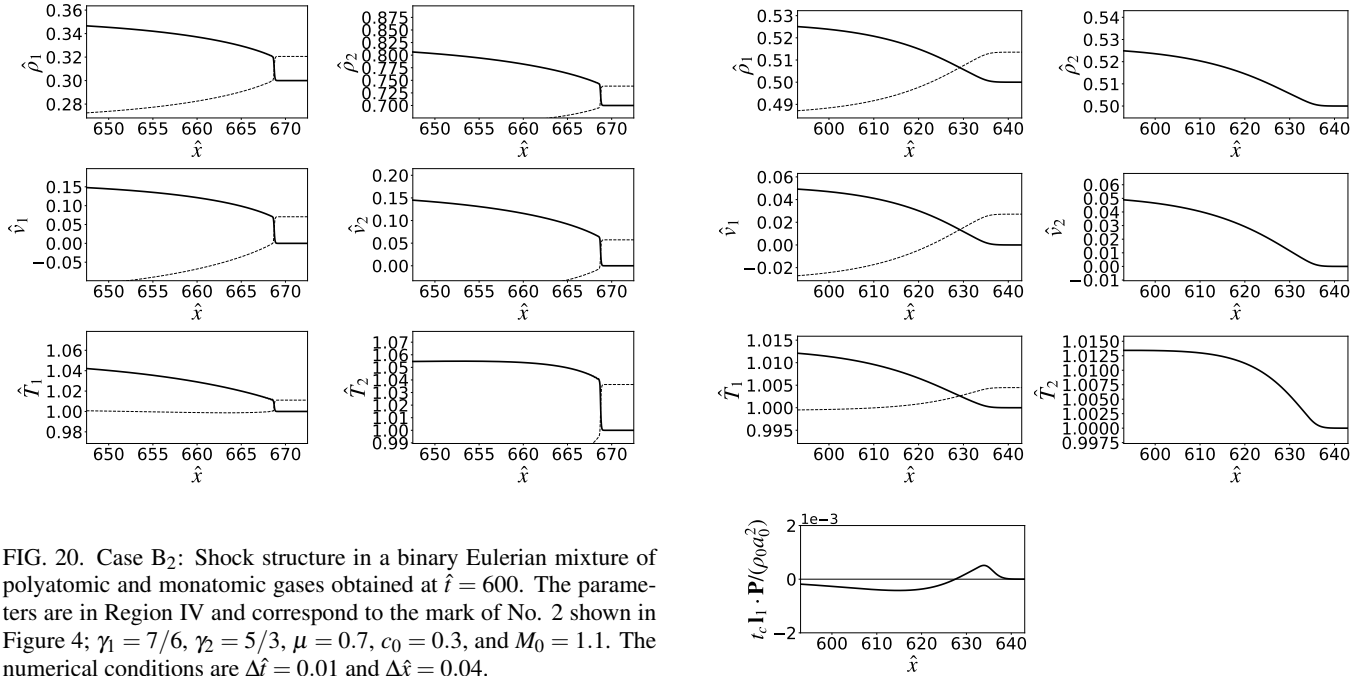


FIG. 20. Case B₂: Shock structure in a binary Eulerian mixture of polyatomic and monatomic gases obtained at $\hat{t} = 600$. The parameters are in Region IV and correspond to the mark of No. 2 shown in Figure 4; $\gamma_1 = 7/6$, $\gamma_2 = 5/3$, $\mu = 0.7$, $c_0 = 0.3$, and $M_0 = 1.1$. The numerical conditions are $\Delta\hat{t} = 0.01$ and $\Delta\hat{x} = 0.04$.

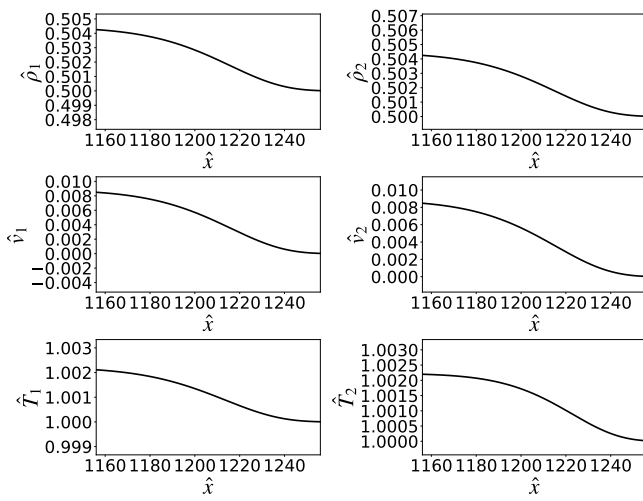


FIG. 21. Case B₃: Shock structure in a binary Eulerian mixture of polyatomic and monatomic gases obtained at $\hat{t} = 1200$. The parameters are in Region I and correspond to the mark of No. 1 shown in Figure 5; $\gamma_1 = 7/6$, $\gamma_2 = 5/3$, $\mu = 0.81$, $c_0 = 0.5$, and $M_0 = 1.005$. The numerical conditions are $\Delta\hat{t} = 0.04$ and $\Delta\hat{x} = 0.16$.

see that the singular point becomes regular singular and the shock-structure solution is continuous. Furthermore, this regular singular point becomes singular and a sub-shock for constituent 1 appears if we increase the Mach number more and we observe multiple sub-shocks for $M_0 = 1.1$ shown in Figure 23.

FIG. 22. Case B₃: Shock structure in a binary Eulerian mixture of polyatomic and monatomic gases obtained at $\hat{t} = 600$. The parameters are in Region IV and correspond to the mark of No. 2 shown in Figure 5; $\gamma_1 = 7/6$, $\gamma_2 = 5/3$, $\mu = 0.81$, $c_0 = 0.5$, and $M_0 = 1.03$. The numerical conditions are $\Delta\hat{t} = 0.02$ and $\Delta\hat{x} = 0.08$.

G. Discontinuity wave induced by a sub-shock

From the profiles of the shock structure with a sub-shock, we notice that the derivative of the physical quantities for a constituent jumps when a sub-shock appears in the other constituent. In other words, a sub-shock for a constituent induces a discontinuity wave for the other constituent. In this section, we derive the relationship between these waves explicitly.

For analyzing the discontinuity wave, it is convenient to rewrite the system of field equations (7) in the following form:

$$\begin{aligned}
& \dot{\rho}_1 + \rho_1 \frac{\partial v_1}{\partial x} = 0, \\
& \rho_1 \dot{v}_1 + \frac{\partial p_1}{\partial x} = \hat{m}_1, \\
& \rho_1 \dot{e}_1 + p_1 \frac{\partial v_1}{\partial x} = \hat{e}_1 - \hat{m}_1 u_1, \\
& \dot{\rho}_2 + \rho_2 \frac{\partial v_2}{\partial x} = 0, \\
& \rho_2 \dot{v}_2 + \frac{\partial p_2}{\partial x} = -\hat{m}_1, \\
& \rho_2 \dot{e}_2 + p_2 \frac{\partial v_2}{\partial x} = -\hat{e}_1 + \hat{m}_1 u_2,
\end{aligned} \tag{50}$$

where a dot on physical quantities represents the material time derivative and in the present case $\dot{X}_\alpha = (\partial X_\alpha / \partial t) + v_\alpha (\partial X_\alpha / \partial x)$ holds with X_α being a generic quantity for the constituent $\alpha = 1, 2$. We introduce $[[X_\alpha]]$ to represent the jump

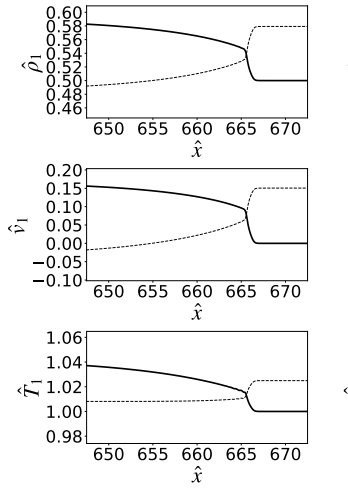


FIG. 23. Case B₃: Shock structure in a binary Eulerian mixture of polyatomic and monatomic gases obtained at $\hat{t} = 600$. The parameters are in Region IV and correspond to the mark of No. 3 shown in Figure 5; $\gamma_1 = 7/6$, $\gamma_2 = 5/3$, $\mu = 0.81$, $c_0 = 0.5$, and $M_0 = 1.1$. The numerical conditions are $\Delta\hat{t} = 0.02$ and $\Delta\hat{x} = 0.08$.

of a generic variable X_α across a sub-shock. Let us consider the case that a sub-shock arise in the constituent 2 ($\llbracket X_2 \rrbracket \neq 0$) and calculate the jump of the derivative of the physical quantities of the constituent 1 ($\llbracket (\partial X_1)/(\partial \varphi) \rrbracket \neq 0$). We introduce $\delta = \llbracket \partial/\partial \varphi \rrbracket$ and by taking the fact that the acceleration wave propagates with the velocity of the shock s into account, the formal substitutions are given by

$$\begin{aligned} \llbracket X_1 \rrbracket = 0, \quad & \left[\left[\frac{\partial X_1}{\partial t} \right] \right] \rightarrow -s\delta X_1, \\ \left[\left[\frac{\partial X_1}{\partial x} \right] \right] \rightarrow \delta X_1, \quad & \llbracket \dot{X}_1 \rrbracket \rightarrow -(s - v_1)\delta X_1. \end{aligned} \quad (51)$$

Subtracting both sides of (50)₁₋₃ and applying the formal substitutions (51), we have

$$\begin{aligned} \delta\rho_1 &= -\frac{m_1 [(\gamma_1 - 1)\llbracket \hat{e}_1 \rrbracket - (\gamma_1 - 1)\llbracket \hat{m}_1 u_1 \rrbracket + (s - v_1)\llbracket \hat{m}_1 \rrbracket]}{m_1(s - v_1)^3 - \gamma_1 k_B T_1(s - v_1)}, \\ \delta v_1 &= -\frac{m_1 [(\gamma_1 - 1)\llbracket \hat{e}_1 \rrbracket - (\gamma_1 - 1)\llbracket \hat{m}_1 u_1 \rrbracket + (s - v_1)\llbracket \hat{m}_1 \rrbracket]}{\rho_1 [m_1(s - v_1)^2 - k_B \gamma_1 T_1]}, \\ \delta T_1 &= -\frac{m_1(\gamma_1 - 1)}{k_B \rho_1(s - v_1) [m_1(s - v_1)^2 - k_B \gamma_1 T_1]} \\ &\times \{ [m_1(s - v_1)^2 - k_B T_1] (\llbracket \hat{e}_1 \rrbracket - \llbracket \hat{m}_1 u_1 \rrbracket) + k_B T_1(s - v_1)\llbracket \hat{m}_1 \rrbracket \}. \end{aligned} \quad (52)$$

We confirm the validity of the expressions (52) in the following way. First, we estimate the strength of the sub-shock appearing in constituent 2 from the shock structure obtained numerically with the use of (49). Then, by inserting the estimated values of the jump of the physical quantities in the constituent 2 into (52), we obtain the derivative for the constituent 1 and plot the theoretical line in addition to the shock structure. In this step, we need to pay attention that, accord-

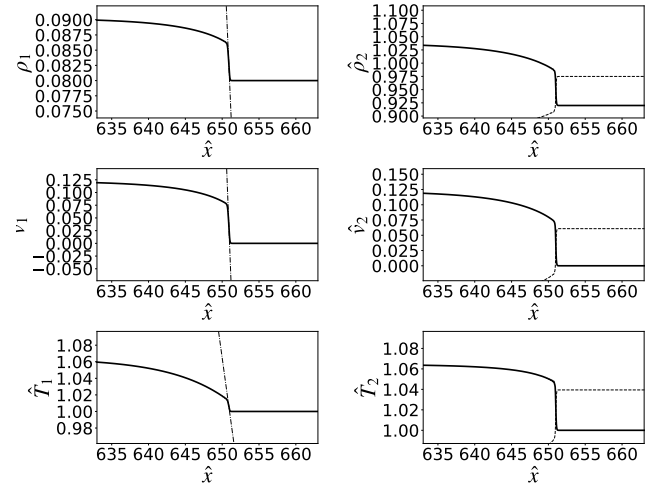


FIG. 24. Shock structure obtained at $\hat{t} = 600$. $\gamma_1 = 7/6$, $\gamma_2 = 5/3$, $\mu = 0.81$, $c_0 = 0.08$, $M_0 = 1.08$, $\Delta\hat{t} = 0.02$, and $\Delta\hat{x} = 0.08$. The dashed line shown in the profile for the constituent 1 represent the theoretical predictions of the derivative of the discontinuity wave. The dotted curves for the constituent 2 are the potential sub-shock predicted any point of the shock structure.

ing to the conjecture on the large-time behavior of the Riemann problem, the derivative with respect to x obtained by the numerical calculation after a long time is the same with the derivative with respect to φ .

Figure 24 shows a typical example of the discontinuity wave for the constituent 1 induced by a sub-shock emerging in the constituent 2. We see that the jump of the derivative of the constituent 1 can be explained by the relationship (52). To the author's knowledge, although the discontinuity waves can be observed numerically in other systems reported in previous papers on the shock structure^{9,12-15}, this is the first case to explain it quantitatively. For completeness, we summarize the expression of the jump of the derivative in the discontinuous wave for constituent 2 in terms of the jump of the physical quantities due to the sub-shock for constituent 1 obtained in a similar way:

$$\begin{aligned} \delta\rho_2 &= \frac{m_2 [(\gamma_2 - 1)\llbracket \hat{e}_2 \rrbracket - (\gamma_2 - 1)\llbracket \hat{m}_2 u_2 \rrbracket + (s - v_2)\llbracket \hat{m}_2 \rrbracket]}{m_2(s - v_2)^3 - \gamma_2 k_B T_2(s - v_1)}, \\ \delta v_2 &= \frac{m_2 [(\gamma_2 - 1)\llbracket \hat{e}_2 \rrbracket - (\gamma_2 - 1)\llbracket \hat{m}_2 u_2 \rrbracket + (s - v_2)\llbracket \hat{m}_2 \rrbracket]}{\rho_2 [m_2(s - v_2)^2 - k_B \gamma_2 T_2]}, \\ \delta T_2 &= \frac{m_2(\gamma_2 - 1)}{k_B \rho_2(s - v_2) [m_2(s - v_2)^2 - k_B \gamma_2 T_2]} \\ &\times \{ [m_2(s - v_2)^2 - k_B T_2] (\llbracket \hat{e}_2 \rrbracket - \llbracket \hat{m}_2 u_2 \rrbracket) + k_B T_2(s - v_2)\llbracket \hat{m}_2 \rrbracket \}. \end{aligned}$$

H. Profiles of the global quantities and average temperature

Because it is quite difficult to measure the profile for each constituent independently, the profiles of averaged or total quantities are often observed experimentally. To understand the shock structure for averaged or total quantities, we need to

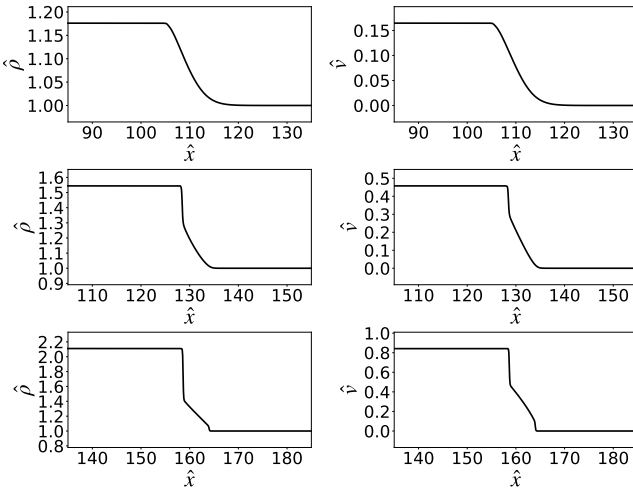


FIG. 25. Case A: Profiles of the dimensionless total mass density and the mixture velocity. The parameters are $\gamma_1 = 7/5$, $\gamma_2 = 9/7$, $\mu = 0.45$, $c_0 = 0.2$. The Mach numbers are $M_0 = 1.1$ (top), $M_0 = 1.3$ (middle), and $M_0 = 1.6$ (bottom).

analyze how the sub-shocks appearing for each constituent affect the profile of these quantities. By using the definitions (3) and (6), we can easily obtain the profiles of the total mass density and the mixture velocity from the ones of the mass densities and the velocity for both constituents. Figure 25 shows the total mass density and the mixture velocity profile corresponding to the parameters adopted in Figures 7-9. Now the meaning of the multiple sub-shocks becomes clear because the two jumps appear in a profile of the total mass density or the mixture velocity for $M_0 = 1.6$ corresponding to Region IV.

Ruggeri and Simić in the paper³⁸ proposed two possible definition of average temperature. The first is based on the idea that the global equation of the energy (8)₃ as in single fluids govern the evolution of the average temperature and for homogeneous solutions (independent of x), the internal energy ε together with Θ become constant (see ref.^{38,39}). Therefore taking into account the expression of the global internal energy (9)₃ we have the average temperature Θ implicitly defined by:

$$\begin{aligned} & \rho_1 \varepsilon_1(\rho_1, \Theta) + \rho_2 \varepsilon_2(\rho_2, \Theta) \\ &= \rho_1 \varepsilon_1(\rho_1, T_1) + \rho_2 \varepsilon_2(\rho_2, T_2) + \frac{1}{2} \rho_1 u_1^2 + \frac{1}{2} \rho_2 u_2^2. \end{aligned} \quad (53)$$

Another possible definition is to consider the identification of the average temperature \mathcal{T} such that the intrinsic internal energy ε_I of the multi-temperature mixture resembles the structure of intrinsic internal energy of a single-temperature one. Therefore, the following implicit definition of an average temperature is adopted:

$$\begin{aligned}\rho \mathcal{E}_I &= \rho_1 \mathcal{E}_1(\rho_1, \mathcal{T}) + \rho_2 \mathcal{E}_2(\rho_2, \mathcal{T}) \\ &= \rho_1 \mathcal{E}_1(\rho_1, T_1) + \rho_2 \mathcal{E}_2(\rho_2, T_2).\end{aligned}\quad (54)$$

If the diffusion is not big so that the process is not far from equilibrium, we may neglect the non-linear terms in (53) and

have $\Theta \simeq \mathcal{T}$. The definition of \mathcal{T} was reconsidered in successive papers^{21,40,41} and, in particular, in²¹, it is proved that \mathcal{T} is the natural definition such that the entropy density is maximum in an equilibrium state.

By inserting the caloric equation of state (1)₂ into (53), we obtain the explicit expression of Θ :

$$\Theta = \frac{\frac{k_B}{m_1} \frac{\rho_1 T_1}{(\gamma_1 - 1)} + \frac{k_B}{m_2} \frac{\rho_2 T_2}{(\gamma_2 - 1)} + \frac{1}{2} \rho_1 u_1^2 + \frac{1}{2} \rho_2 u_2^2}{k_B \left\{ \frac{\rho_1}{m_1(\gamma_1 - 1)} + \frac{\rho_2}{m_2(\gamma_2 - 1)} \right\}}. \quad (55)$$

or

$$\Theta = \frac{\frac{k_B}{m_1} \frac{\rho_1 T_1}{(\gamma_1 - 1)} + \frac{k_B}{m_2} \frac{\rho_2 T_2}{(\gamma_2 - 1)} + \frac{1}{2}(\Pi - \sigma)}{k_B \left\{ \frac{\rho_1}{m_1(\gamma_1 - 1)} + \frac{\rho_2}{m_2(\gamma_2 - 1)} \right\}}. \quad (56)$$

While \mathcal{T} becomes:

$$\mathcal{T} = \frac{\frac{1}{m_1} \frac{\rho_1 T_1}{(\gamma_1 - 1)} + \frac{1}{m_2} \frac{\rho_2 T_2}{(\gamma_2 - 1)}}{\frac{\rho_1}{m_1(\gamma_1 - 1)} + \frac{\rho_2}{m_2(\gamma_2 - 1)}}. \quad (57)$$

For convenience, we introduce the dimensionless average temperature $\hat{\Theta} \equiv \Theta/T_0$:

$$\hat{\Theta} = \frac{\frac{\hat{\rho}_1 \hat{T}_1}{(\gamma_1 - 1)} + \mu \frac{\hat{\rho}_2 \hat{T}_2}{(\gamma_2 - 1)} + \frac{1}{2} \gamma_0 \frac{m_1}{m_0} \left\{ \hat{\rho}_1 (\hat{v}_1 - \hat{v})^2 + \hat{\rho}_2 (\hat{v}_2 - \hat{v})^2 \right\}}{\frac{\hat{\rho}_1}{(\gamma_1 - 1)} + \mu \frac{\hat{\rho}_2}{(\gamma_2 - 1)}}, \quad (58)$$

where taking into account (5) m_1/m_0 can be written as

$$\frac{m_1}{m_0} = c_0 + \mu(1 - c_0). \quad (59)$$

The dimensionless form of $\hat{\mathcal{T}} \equiv \mathcal{T}/T_0$ is given by

$$\hat{\mathcal{J}} = \frac{\frac{\hat{\rho}_1 \hat{T}_1}{(\gamma_1 - 1)} + \mu \frac{\hat{\rho}_2 \hat{T}_2}{(\gamma_2 - 1)}}{\left\{ \frac{\hat{\rho}_1}{(\gamma_1 - 1)} + \mu \frac{\hat{\rho}_2}{(\gamma_2 - 1)} \right\}}. \quad (60)$$

We show the profile of the average temperature Θ and \mathcal{T} in Figure 26 with the parameters corresponding to the ones in Figures 7-9 and also in Figure 27 with the parameters corresponding to the ones in Figures 10 and 11. It is confirmed that the sub-shock formation can also be detected through the measurement of the average temperature. While the difference between Θ and \mathcal{T} is negligible for small Mach numbers, the nonlinear terms may play a role in the profile of the average temperature for large Mach numbers.

VI. SUMMARY AND CONCLUDING REMARKS

In the present paper, we have analyzed the shock structure in a binary Eulerian mixture of gases with different degrees of freedom by using the framework of the multi-temperature model. In the first part, by considering the necessary conditions of the sub-shock formation, we have classified the possible regions for the sub-shock formation into four parts in

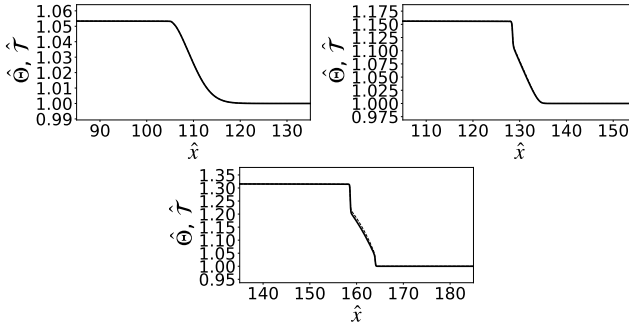


FIG. 26. Profiles of the dimensionless average temperature $\hat{\Theta}$ (solid curve) and \hat{T} (dotted curve). $\gamma_1 = 7/5$, $\gamma_2 = 9/7$, $\mu = 0.45$, and $c_0 = 0.2$. The Mach numbers are $M_0 = 1.1$ (above left), $M_0 = 1.3$ (above right), and $M_0 = 1.6$ (below).

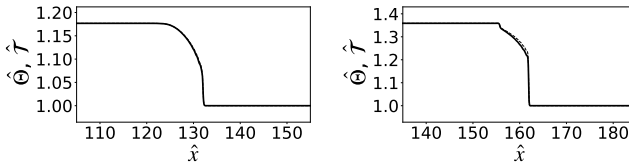


FIG. 27. Profiles of the dimensionless average temperature $\hat{\Theta}$ (solid curve) and \hat{T} (dotted curve). $\gamma_1 = 7/5$, $\gamma_2 = 9/7$, $\mu = 0.45$, and $c_0 = 0.6$. The Mach numbers are $M_0 = 1.3$ (left) and $M_0 = 1.6$ (right).

terms of the concentration and the Mach number. It is found that the topology of the regions can be quite different from the one obtained in a binary mixture of monatomic gases if the degrees of freedom of a lighter molecule is larger than the one of a heavier molecule. In the second part, we have numerically solved the system of field equations and have made the possibility of the sub-shock formation clear for all cases of the parameters in the classified regions. Moreover, we have found that a regular singular point for moderate Mach numbers may become singular for larger Mach numbers. The relationship between the sub-shock for a constituent and the acceleration wave for the other constituent is explicitly derived. From the viewpoint of possible experimental observation, we have also shown the shock structure for the global or average quantities, in particular, the one for the average temperature.

The remarks of the present study are summarized as follows:

(I) We need to pay attention to the fact that the present analysis is based on the Eulerian mixture of polyatomic gases in which the viscosity and heat conductivity of each constituent are neglected. In reality, the sub-shock (discontinuous surface) does not exist, and it is replaced by a steep but continuous change in the physical quantity. Nevertheless, the thickness of the shock is for many gases, particularly for monatomic gas of the order of mean free path and therefore negligible at the macroscopic scale. The previous observation agrees that the shock wave theory based on the system of Euler equations in a single fluid has vast literature. We could not find experimental data for the binary mixture to compare

our results. For possible future experimental verification of the corresponding phenomena found in the present paper, it is essential to choose a pair of gases with appropriate degrees of freedom and the ratio of the masses. We summarize the values of γ_1 , γ_2 , and μ for possible pairs of gases classified into cases A and B in Tables I and II.

TABLE I. Values of the ratio of the specific heats at 298.15 [K] and the ratio of the masses⁴² for typical binary mixtures of gases in Case A.

	γ_1	γ_2	μ	μ^*
He / CO ₂	5/3	1.29	0.091	0.259
H ₂ / CO ₂	1.41	1.29	0.046	0.157
N ₂ / CO ₂	1.40	1.29	0.637	0.155

TABLE II. Values of the ratio of the specific heats at 298.15 [K] and the ratio of the masses⁴² for typical binary mixtures of gases in Case B.

	γ_1	γ_2	μ	g	μ^{**}
N ₂ / Ar	1.40	5/3	0.701	0.840	0.897
O ₂ / Ar	1.39	5/3	0.801	0.837	0.897
HCl / Ar	1.40	5/3	0.913	0.836	0.897

(II) The sub-shock formation plays an essential role in the context of the shock structure in a single fluid of some rarefied polyatomic gases that have a large bulk viscosity⁴³⁻⁴⁵. The theory of mixtures of polyatomic gases with large bulk viscosity based on the RET theory has been proposed⁴⁶ and we will consider in a future paper the shock structure in a binary mixture incorporating the effect of the dynamic pressure.

ACKNOWLEDGMENTS

This work is partially supported by GNFM- INdAM (TR) and by JSPS KAKENHI Grant Number JP19K04204 (ST).

AUTHOR DECLARATIONS

CONFLICT OF INTEREST

The authors have no conflicts to disclose.

DATA AVAILABILITY

Data sharing is not applicable to this article as no new data were created or analyzed in this study.

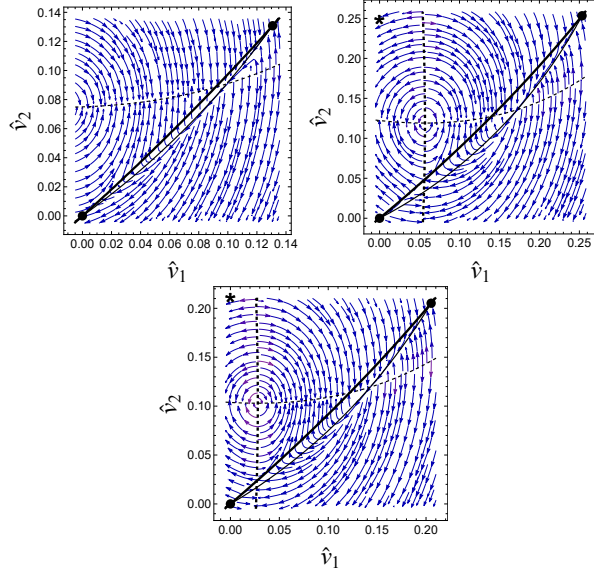


FIG. 28. Direction fields in the case of $\gamma_1 = 7/6$, $\gamma_2 = 5/3$, $\mu = 0.55$ and $c_0 = 0.57$ for $M_0 = 1.075$ (above left), 1.12 (below), 1.15 (above right). The curves of $M_0 = M_{10}$ (thick dashed curve), $M_0 = M_{20}$ (thin dashed curve), $(dv_1)/(d\varphi) = 0$ (thick solid curve) and $(dv_2)/(d\varphi) = 0$ (thick solid curves) are also shown. The black marks represent the unperturbed and unperturbed states and the star is the state just after a sub-shock s_1^A .

Appendix A: Dynamical analysis of the ODE system

In this section, we summarize a method to classify the shock-structure solutions numerically from the viewpoint of the dynamical analysis of the ODE system (20). In the present case, the ODE system (20) is written in the following explicit form with the independent variables $\mathbf{u} = (\rho_1, \rho_2, v_1, v_2, T_1, T_2)$:

$$\begin{aligned}
 \frac{d}{d\varphi} (-s\rho + \rho v) &= 0, \\
 \frac{d}{d\varphi} (-s\rho v + \rho v^2 + p + \Pi - \sigma) &= 0, \\
 \frac{d}{d\varphi} \left\{ -s \left(\frac{1}{2} \rho v^2 + \rho \varepsilon \right) + \left(\frac{1}{2} \rho v^2 + \rho \varepsilon + p + \Pi - \sigma \right) v + q \right\} &= 0, \\
 \frac{d}{d\varphi} (-s\rho_1 + \rho_1 v_1) &= 0, \\
 \frac{d}{d\varphi} (-s\rho_1 v_1 + \rho_1 v_1^2 + p_1) &= \hat{m}_1, \\
 \frac{d}{d\varphi} \left\{ -s (\rho_1 v_1^2 + 2\rho_1 \varepsilon_1) + (\rho_1 v_1^2 + 2\rho_1 \varepsilon_1 + 2p_1) v_1 \right\} &= 2(\hat{e}_1 + \hat{m}_1 v),
 \end{aligned} \tag{A1}$$

where (9), (12) and (11) hold. We can immediately integrate (A1)_{1–4} and obtain the expressions of ρ_1 , ρ_2 , T_1 and T_2 in terms of v_1 and v_2 . By inserting the obtained expressions into (A1)_{1–4}, we have

$$\begin{aligned}
 \frac{dv_1}{d\varphi} &= f_1(v_1, v_2), \\
 \frac{dv_2}{d\varphi} &= f_2(v_1, v_2).
 \end{aligned}$$

Although the functional forms of f_1 and f_2 are too complicated to write down here explicitly, we can draw the direction

fields for the corresponding shock-structure solution numerically.

Figures 28 shows the direction fields in the case of $\gamma_1 = 7/6$, $\gamma_2 = 5/3$, $\mu = 0.55$ and $c_0 = 0.57$. The Mach numbers are adopted $M_0 = 1.075$, 1.12, and 1.15, respectively. In this figure, we show the state just after the sub-shock s_1^A and the curves of $M_0 = M_{10}$, $M_0 = M_{20}$, $(dv_1)/(d\varphi) = 0$ and $(dv_2)/(d\varphi) = 0$. The shock structure solution connecting two equilibrium state pass the meeting point between the curves of $M_0 = M_{20}$ and of $(dv_2)/(d\varphi) = 0$ for $M_0 = 1.075$. Therefore the solution becomes continuous as we see in Figure 17. In the case of $M_0 = 1.15$, the Mach number is larger

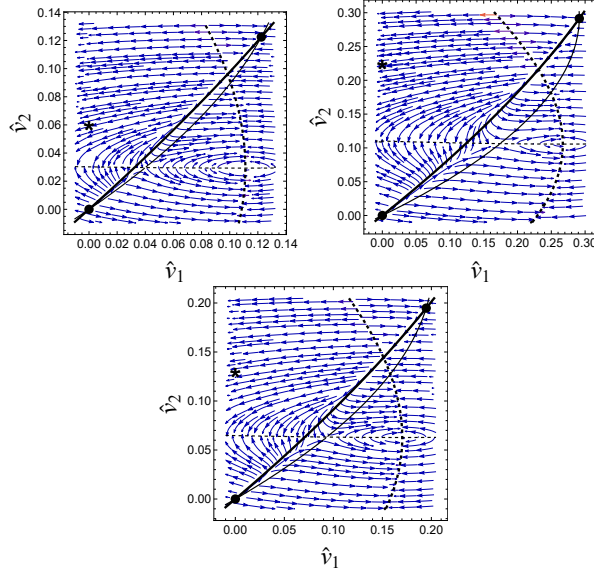


FIG. 29. Direction fields in the case of $\gamma_1 = 7/6$, $\gamma_2 = 5/3$, $\mu = 0.81$ and $c_0 = 0.08$ for $M_0 = 1.08$ (above left), 1.13 (below), 1.2 (above right). The curves of $M_0 = M_{10}$ (thick dashed curve), $M_0 = M_{20}$ (thin dashed curve), $(dv_1)/(d\varphi) = 0$ (thick solid curve) and $(dv_2)/(d\varphi) = 0$ (thick solid curves) are also shown. The black marks represent the unperturbed and unperturbed states and the star is the state just after a sub-shock s_2^A .

than the maximum characteristic velocity, and the solution should be connected with the state just after the sub-shock s_1^A . However, as we see from Figure 17, the solution does not cross the meeting point between the curves of $M_0 = M_{20}$ and of $(dv_2)/(d\varphi) = 0$. This fact implies that the sub-shock should emerge. In such a way, we can interpret the behavior of the shock-structure solution without solving the Riemann problem and identify the critical Mach number as $M_0 \simeq 1.12$ by searching a threshold value such that the solution passes the meeting point between the curves of $M_0 = M_{20}$ and of $(dv_2)/(d\varphi) = 0$.

Figures 28 shows the direction fields in the case of $\gamma_1 = 7/6$, $\gamma_2 = 5/3$, $\mu = 0.81$ and $c_0 = 0.08$ for $M_0 = 1.08, 1.13$, and 1.2 . As all $M_0 = 1.08, 1.13, 1.2$ are larger than M_{20} , a sub-shock for constituent 2 emerges. In a similar way, we can identify the boundary is $M_0 \simeq 1.13$ also in Case B.

¹W.G. Vincenti and C.H. Kruger, Jr., *Introduction to Physical Gas Dynamics* (John Wiley and Sons, New York, London, Sydney, 1965).

²Ya. B. Zel'dovich and Yu. P. Raizer, *Physics of Shock Waves and High-Temperature Hydrodynamic Phenomena* (Dover Publications, Mineola, New York, 2002).

³T. Ruggeri and S. Taniguchi, "Shock Waves in Hyperbolic Systems of Non-Equilibrium Thermodynamics," in *Applied Wave Mathematics II* edited by A. Berezovski and T. Soomere (Springer, Cham, 2019) pp. 167 - 186.

⁴T.-P. Liu, *Shock Waves*, Graduate Studies in Mathematics 215, American Mathematical Society (AMS), Providence (2020)

⁵T. Ruggeri, "Breakdown of shock-wave-structure solutions," *Phys. Rev. E* **47**, 4135 (1993).

⁶G. Boillat and T. Ruggeri, "On the shock structure problem for hyperbolic system of balance laws and convex entropy," *Cont. Mech. Thermodyn.* **10** (1998) 285–292.

- ⁷I. Müller and T. Ruggeri, *Rational Extended Thermodynamics*. 2nd ed. (Springer, New York, 1998).
- ⁸W. Weiss, "Continuous shock structure in extended thermodynamics," *Phys. Rev. E* **52**, R5760 (1995).
- ⁹S. Taniguchi and T. Ruggeri, "On the sub-shock formation in extended thermodynamics," *Int. J. Non-Linear Mech.* **99**, 69 (2018).
- ¹⁰T. Ruggeri and M. Sugiyama, *Rational Extended Thermodynamics beyond the Monatomic Gas* (Springer, Cham, 2015).
- ¹¹T. Ruggeri and M. Sugiyama, *Classical and Relativistic Rational Extended Thermodynamics of Gases* (Springer, Cham, 2021).
- ¹²F. Conforto, A. Mentrelli, and T. Ruggeri, "Shock structure and multiple sub-shocks in binary mixtures of Eulerian fluids," *Ricerche di Matematica* **66**, 221 (2017).
- ¹³M. Bisi, G. Martalò, and G. Spiga, "Shock wave structure of multi-temperature Euler equations from kinetic theory for a binary mixtures" *Acta Appl. Math.* **132**, 95 (2014).
- ¹⁴V. Artale, F. Conforto, G. Martalò, and A. Ricciardello, "Shock structure and multiple sub-shocks in Grad 10-moment binary mixtures of monatomic gases," *Ricerche di Matematica* **68**, 485 (2019).
- ¹⁵S. Taniguchi and T. Ruggeri, "A 2×2 simple model in which the sub-shock exists when the shock velocity is slower than the maximum characteristic velocity," *Ricerche di Matematica* **68**, 167 (2019).
- ¹⁶T. Ruggeri and S. Simić, "On the hyperbolic system of a mixture of Eulerian fluids: a comparison between single- and multi-temperature models," *Mathematical Methods in the Applied Sciences* **30**, 827 (2007).
- ¹⁷S. Simić and T. Ruggeri, "Shock structure in a hyperbolic model of binary mixture of non-reacting gases," in *Proceedings of First Serbian (26th YU) Congress on Theoretical and Applied Mechanics*, pp. 237-246. Published by Serbian Society of Mechanics, Belgrade, ISBN 978-86-909973 (2007).
- ¹⁸D. Madjarević, T. Ruggeri, and S. Simić, "Shock structure and temperature overshoot in macroscopic multi-temperature model of mixtures," *Phys. Fluids* **26**, 106102 (2014).
- ¹⁹D. Madjarević, and S. Simić, "Shock structure in helium-argon mixture —A comparison of hyperbolic multi-temperature model with experiment," *EPL* **102**, 44002 (2013).
- ²⁰T. Ruggeri and S. Taniguchi, "Sub-shock formation in shock structure of a binary mixture of polyatomic gases," *Atti Accad. Naz. Lincei Cl. Sci. Fis. Mat. Natur.* **32**, 167 (2021).
- ²¹T. Ruggeri and S. Simić, "Average temperature and Maxwellian iteration in multitemperature mixtures of fluids," *Phys. Rev. E* **80**, 026317 (2009).
- ²²G. Boillat and T. Ruggeri, "Hyperbolic principal subsystems: Entropy convexity and subcharacteristic conditions," *Arch. Rat. Mech. Anal.* **137**, 305 (1997).
- ²³P. D. Lax, "Hyperbolic systems of conservation laws II," *Comm. Pure Appl. Math.* **10**, 537 (1957).
- ²⁴T. Ruggeri, A. Muracchini, and L. Seccia, "Continuum approach to phonon gas and shape changes of second sound via shock wave theory," *Nuovo Cimento D* **16**, 15 (1994).
- ²⁵T. Bose, *High Temperature Gas Dynamics* (Springer, Berlin, 2004).
- ²⁶M. Pavić-Čolić, "Multi-velocity and multi-temperature model of the mixture of polyatomic gases issuing from kinetic theory," *Phys. Lett. A* **383**, 2829 (2019).
- ²⁷D. Madjarević, M. Pavić-Čolić, and S. Simić, "Shock structure and relaxation in the multi-component mixture of Euler fluids," *Symmetry* **13**, 955 (2021).
- ²⁸T.-P. Liu, "Linear and nonlinear large-time behavior of solutions of general systems of hyperbolic conservation laws," *Commun. Pure Appl. Math.* **30**, 767 (1977).
- ²⁹T.-P. Liu, "Large-time behavior of solutions of initial and initial-boundary value problems of a general system of hyperbolic conservation laws," *Commun. Math. Phys.* **55**, 163 (1977).
- ³⁰F. Brini and T. Ruggeri, "On the Riemann problem in extended thermodynamics," in *Proceedings of the 10th International Conference on Hyperbolic Problems (HYP2004), Osaka, 13–17 Sept 2004*, vol. I, (Yokohama Publisher Inc., Yokohama, 2006) pp. 319–326.
- ³¹F. Brini and T. Ruggeri, "On the Riemann problem with structure in extended thermodynamics," *Suppl. Rend. Circ. Mat. Palermo II* **78**, 31 (2006).
- ³²A. Mentrelli and T. Ruggeri, "Asymptotic behavior of Riemann and Riemann with structure problems for a 2×2 hyperbolic dissipative system," *Suppl. Rend. Circ. Mat. Palermo II* **78**, 201 (2006).

³³T.-P. Liu, “Nonlinear hyperbolic-dissipative partial differential equations,” in *Recent Mathematical Methods in Nonlinear Wave Propagation, Lecture Notes in Mathematics*, vol. 1640, edited by T. Ruggeri (Springer, Berlin, 1996) pp. 103-136.

³⁴E. Toro, *Riemann Solvers and Numerical Methods for Fluid Dynamics*, (Springer, Berlin, 2009).

³⁵F. Brini and T. Ruggeri, “The Riemann problem for a binary non-reacting mixture of Euler fluids,” in *Proceedings XII Int. Conference on Waves and Stability in Continuous Media*, edited by R. Monaco, et al. (World Scientific, Singapore, 2004) pp. 102-108.

³⁶S. F. Liotta, V. Romano, and G. Russo, “Central schemes for balance laws of relaxation type,” *SIAM J. Numer. Anal.* **38**, 1337 (2000).

³⁷P. Virtanen, R. Gommers, T. E. Oliphant, M. Haberland, T. Reddy, D. Cournapeau, E. Burovski, P. Peterson, W. Weckesser, J. Bright, S. J. van der Walt, M. Brett, J. Wilson, K. J. Millman, N. Mayorov, A. R. J. Nelson, E. Jones, R. Kern, E. Larson, CJ Carey, I. Polat, Y. Feng, E. W. Moore, J. VanderPlas, D. Laxalde, J. Perktold, R. Cimrman, I. Henriksen, E.A. Quintero, C. R Harris, A. M. Archibald, A. H. Ribeiro, F. Pedregosa, P. van Mulbregt, and SciPy 1.0 Contributors, “SciPy 1.0: Fundamental Algorithms for Scientific Computing in Python,” *Nature Methods*, **17**, 261 (2020).

³⁸T. Ruggeri and S. Simić, “Mixture of gases with multi-temperature: Identification of a macroscopic average temperature,” *Memorie dell’Accademia delle Scienze, Lettere ed Arti di Napoli, Proceedings Mathematical Physics Models and Engineering Sciences*, pp. 455-465 (2008): [http://www.societanazionalecienzeletterearti.it/pdf/Memorie%20SFM%20-%20Mathematical%20Physics%20Model%20\(2008\).pdf](http://www.societanazionalecienzeletterearti.it/pdf/Memorie%20SFM%20-%20Mathematical%20Physics%20Model%20(2008).pdf)

³⁹S.-Y. Ha and T. Ruggeri, “Emergent dynamics of a thermodynamically consistent particle model,” *Arch. Ration. Mech. Anal.* **223**, 1397 (2017).

⁴⁰H. Gouin and T. Ruggeri, “Identification of an average temperature and a dynamical pressure in a multitemperature mixture of fluids,” *Phys. Rev. E* **78**, 016303 (2008).

⁴¹T. Ruggeri and J. Lou, “Heat conduction in multi-temperature mixtures of fluids: the role of the average temperature,” *Physics Lett. A* **373**, 3052 (2009).

⁴²W. M. Haynes (eds), *CRC Handbook of Chemistry and Physics, 95th ed.* (CRC Press, Boca Raton, FL, 2014).

⁴³S. Taniguchi, T. Arima, T. Ruggeri, and M. Sugiyama, “Effect of the dynamic pressure on the shock wave structure in a rarefied polyatomic gas,” *Phys. Fluids* **26**, 016103 (2014).

⁴⁴S. Taniguchi, T. Arima, T. Ruggeri, and M. Sugiyama, “Overshoot of the non-equilibrium temperature in the shock wave structure of a rarefied polyatomic gas subject to the dynamic pressure,” *Int. J. Non-Linear Mech.* **79**, 66 (2016).

⁴⁵S. Taniguchi, T. Arima, T. Ruggeri, and M. Sugiyama, “Shock wave structure in rarefied polyatomic gases with large relaxation time for the dynamic pressure,” *Journal of Physics: Conference Series* **1035**, 012009 (2018).

⁴⁶T. Arima, T. Ruggeri, M. Sugiyama, and S. Taniguchi, “Galilean invariance and entropy principle for a system of balance laws of mixture type,” *Atti Accad. Naz. Lincei Cl. Sci. Fis. Mat. Natur.* **28**, 495 (2017).